*Russian Chemical Reviews* **82** (12) 1135 – 1159 (2013) © 2013 Russian Academy of Sciences and Turpion Ltd

DOI 10.1070/RC2013v082n12ABEH004344

# Shape memory effect and superelasticity of titanium nickelide alloys implanted with high ion doses

A D Pogrebnjak, S N Bratushka, V M Beresnev, N Levintant-Zayonts

## Contents


| | | |
|---|---|---|
| I. | Introduction | 1135 |
| II. | Specific features of ion implantation as method for surface modification of materials | 1136 |
| III. | Properties of ion-implanted surface layer | 1138 |
| IV. | The shape memory alloys | 1139 |
| V. | Influence of ion implantation on the structure of NiTi alloys, the shape memory effect and superelasticity | 1144 |
| VI. | Influence of high doses of implanted ions on physicomechanical properties of NiTi alloys | 1150 |
| VII. | Conclusion | 1155 |


**Abstract. The state of the art in ion implantation of superelastic NiTi shape memory alloys is analyzed. Various technological applications of the shape memory effect are outlined. The principles and techiques of ion implantation are described. Specific features of its application for modification of surface layers in surface engineering are considered. Key properties of shape memory alloys and problems in utilization of ion implantation to improve the surface properties of shape memory alloys, such as corrosion resistance, friction coefficient, wear resistance, *etc*. are discussed. The bibliography includes 162 references.**

## I. Introduction

The design of novel materials is a key avenue of scientific research aimed at progress in modern technology. All materials can be classified into structural and functional ones. The latter exhibit specific properties. Metallic alloys that demonstrate the shape memory effect can be treated as materials that simultaneously show the properties of structural and functional materials. An example is provided by titanium nickelide NiTi.† This compound exhibits unique properties called the shape memory effect and superelasticity. In spite of considerable literature on these properties, opinions are different on their mechanisms and on the reasons for and nature of processes occurring in solids at the structural level. Recently, this was clearly demonstrated in a special issue of 'Scripta Materialia' journal[1] devoted to the state of the art in research on shape memory alloys.‡

Most studies on shape memory materials are concerned with formation of surface layers with improved operating properties. This can be done using methods suitable for modification of near-surface layers. As a result, one gets materials with improved operating properties (*e.g*., hardness, elastic modulus, wear resistance, corrosion resistance, *etc*.). The key issue is a correct choice of the modification technique that should provide improved properties in the surface layers of a material and retain the initial superelasticity and shape memory effect. Ion implantation belongs to the most preferable and widely used methods for surface modification of solids including metals, ceramics, semiconductors and polymers. This is confirmed by numerous studies carried out worldwide. Indisputable advantages of the technique are as follows:

— the possibility to make the modified layer as thin as possible with retention of specific features of phase transitions typical of the shape memory effect in the matrix material;

— less probable delamination of coatings (high adhesion of the implanted layer to the matrix) because there is no clear separation between the surface layer and the matrix material;

**A D Pogrebnjak, S N Bratushka** Sumy State University, ul. Rimskogo-Korsakova 2, 40007 Sumy, Ukraine. Tel. (38-0686) 52 96 47, e-mail: alexp@i.ua (A D Pogrebnjak), tel. (38-0966) 96 40 58, e-mail: s_bratushka@mail.ru (S N Bratushka)
**V M Beresnev** V N Karazin Kharkiv National University, pl. Svobody 4, 61077 Kharkiv, Ukraine. Tel. (38-0506) 41 60 35, e-mail: Beresnev-scpt@yandex.ru
**N Levintant-Zayonts** Institute of Fundamental Technological Research Polish Academy of Sciences, ul. Pawinskiego 5B, 02-106 Warsaw, Poland. Tel. (48-22) 826 12 81, ext. 261, e-mail: neonila@ippt.gov.pl

Received 26 July 2012
*Uspekhi Khimii* **82** (12) 1135 – 1159 (2013); translated by A M Raevskiy

† Intermetallic nickel – titanium alloys are called 'nitinols'.

‡ The Editor's Preface began with the words: 'We invited several researchers presently dealing with this subject to write down, quite literally, their 'viewpoint' on a relevant question pertaining to shape memory alloys... The papers that follow do not always agree: there are conflicting viewpoints, with the obvious implication that at least one cannot be entirely correct.' This points not only to interest in shape memory alloys, but also to the fact that the phenomena and processes occurring in these systems are still to be clarified.

— the possibility to use the technique as surface-doping method and thus significantly influence not only the structure of near-surface layers, but also the properties of the matrix material, *viz*., the characteristic transition temperatures, the superelastic behaviour, the shape memory effect, *etc*.

Among shape memory materials, nickel and titanium alloys are of the greatest importance for industry. The production technology of NiTi alloys has been known since the 1970s; however, processes occurring under operating conditions and on thermomechanical treatment are to be clarified as yet. Therefore, these materials are still subject to numerous studies.

During the last 10–15 years, there has been considerable literature including a variety of collections,[1–5] reviews,[6–9] monographs,[10–15] handbooks[16,17] and original research articles. However, problems in applications of ion implantation and ion-beam modification of NiTi-based materials have not been considered in detail. On the other hand, a number of studies on problems in ion implantation into solids[7–42] include almost no information on ion beam induced modification of the properties of NiTi alloys[43–50] or contain fragmentary results of certain studies carried out without detailed analysis, consideration of the nature and mechanisms of the observed phenomena. Russian researchers and their colleagues from the former USSR have contributed largely to investigations of the shape memory effect and superelasticity. The results of their studies are available from various publications including monographs.[10–17]

To ensure targeted surface modification, to vary the properties of a material in specified manner and to control them, one should consider a broad range of phenomena occurring in a shape memory material representing a complex system 'implanted layer/matrix'. However, it should be noted that such studies are scarce, some results being contradictory.[29–42]

The aim of this review was to present the state of the art in studies on shape memory materials and the potential of high-dose ion implantation in order to improve the physicochemical and mechanical properties of such materials taking NiTi-based alloys as examples.

## II. Specific features of ion implantation as method for surface modification of materials

Numerous publications include the description and analysis of results obtained in studies on various avenues of application of ion implantation technique.[48–100] By and large, the method is used:

— to improve the functional properties of surface and

— to study processes occurring in materials irradiated with high-energy particles.

In essence, ion implantation is a kind of doping materials with high-energy particles. Atoms of the dopant elements are ionized in an ion source and then accelerated in an electric field to have energies from tens to hundreds of keV (this corresponds to ion velocities from hundreds to thousands kilometres per second). The ion beam thus formed is directed to the surface of a material. Ions bombarding the target penetrate the material to a depth of up to 1 μm. Dynamic character of the process means that (i) materials can be doped by almost all elements, (ii) the concentrations of implanted ions can be very high (up to 50 at.% and more) and (iii) the process can be implemented at rather low temperatures.[27,43,44,48–50,52–58]

Two main ion implantation regimes involve continuous and pulsed bombardment of a material. In the former case, high-energy ions continuously penetrate the solid surface of the matrix material. Implanted ions penetrate the material to a depth from 0.01 to 1 μm and gradually lose their energy in the interaction with atoms of the crystal lattice of the matrix material.

A schematic of ion implantation and a typical plot of the concentration of implanted ions ($c_i$) *versus* penetration depth ($l$), also called the concentration profile of dopant ions in the matrix material, are shown in Fig. 1. Noteworthy is a characteristic maximum of concentration, $c_{max}$, located at distance $l_c$ from the surface of the material; at this distance, ions lose their energy and can be treated as being 'at rest'. The $l_c$ value depends on the nature of the solid and implanted ions.[29–32,36,37,51–56,61,71–82,101]

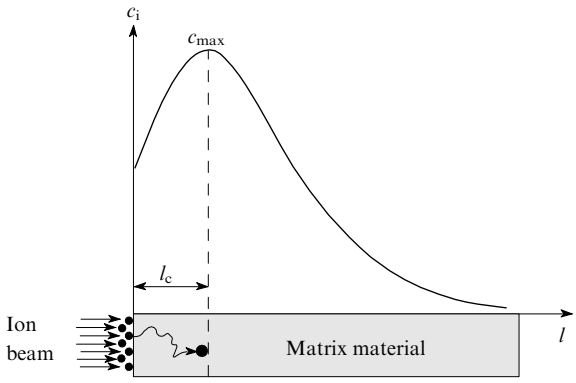



**Fig. 1.** Scheme of ion implantation and the concentration profile of elements implanted in the matrix material.[43]

The volume of the material containing implanted alien ions remains almost unchanged compared to the initial state of the material; therefore, ion implantation is accompanied by development of stress in the near-surface layer.[4,5] This is also observed on local increase in temperature on the surface of the implanted material. According to a thermal peak model, energy dissipation for an individual ion occurs through formation, along the ion trajectory, of a local region a few manometers in size with an initial temperature of nearly 1000 °C and a lifetime no longer than $10^{-11}$ s. Heating of the implanted material first of all depends on the ion dose [number of implanted ions per unit surface area of the matrix material ($D$)], ion energy ($E$) and duration of continuous irradiation. Usually, implantation is implemented in such a manner that the temperature of a material be at most 200 °C in order to avoid irreversible changes in the material.

Low-energy ion implantation is characterized by ion energies of at most 100 keV. In high-energy ion implantation, the ion energies lie between hundreds of keV and a few MeV. Experiments[3,24,44] showed that the higher the ion energy the greater the penetration depth; however, the peak in the concentration profile of the dopant ions becomes more 'diffuse' (Fig. 2 *a*).

Most modern ion implanters operate at low currents and obtaining desired results requires a longer implantation

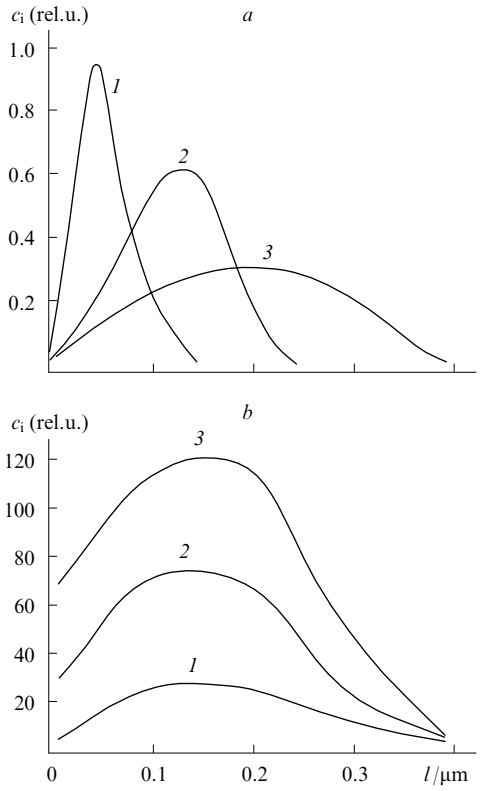



**Fig. 2.** Concentrations of nitrogen ions implanted into steel plotted *vs.* ion energy (*a*) and ion dose (*b*).[62]
Nitrogen ions ($E = 75$ keV) implanted into iron.
(*a*) $E = 50$ (*1*), 100 (*2*), 200 keV (*3*); (*b*) $D = 3 \times 10^{17}$ (*1*), $6 \times 10^{17}$ (*2*), $10^{18}$ (*3*) ion cm$^{-2}$.

time. Therefore, utilization of these devices may appear to be economically unsound. In the case of high-energy beams, ion implanters are used to 'mix' coatings prepared earlier by other methods and thus attain the desired concentration of necessary dopant elements. Note that for complete ion 'mixing' the coating should be implanted with a much lower dose (up to $10^{16}$ ion cm$^{-2}$) compared to the dose needed for direct implantation (up to $10^{18}$ ion cm$^{-2}$).[44, 45, 49, 50, 95]

Practically, ion implantation is used to create dopant concentrations from a few to a few tens of atomic per cent in the near-surface layer. At low doses, the concentration profile of implanted ions obeys a Gauss distribution. Unlike semiconductors, high ion doses from $10^{16}$ to $(1-6) \times 10^{18}$ ion cm$^{-2}$ are needed to impart necessary properties to metals (see Refs 38 – 42, 59, 60, 63 – 70, 91 – 93, 102 – 112). At such doses, atoms in the implanted layer can be several times displaced from their equilibrium positions. The concentration profile of the implanted element is affected by the accompanying processes (ion-beam sputtering of a surface, scattering of the ion beam, ion mixing, segregation of accelerated ions, radiation-accelerated diffusion) resulting in new compounds (phases). In most cases, one or two processes dominate. That is why the concentration profile of dopant ions differs from the classical Gaussian curve.

The concentration profiles of implanted ions in the near-surface layers at high implantation doses and the determination of the size of such layers have been subjects of considerable experimental and theoretical research. Creation of high concentration of dopant elements and great implantation depths by increasing ion beam energy, energy density and ion dose is precluded by sputtering of surface layers of the material. This is a key effect that qualitatively influences the shape of the concentration profile of implanted ions. In some cases, the maximum in the concentration profile can be in the vicinity of the surface; here, the number of implanted ions becomes equal to that of sputtered atoms.[4] This is characteristic of implantation of heavy-element ions.

Modern high-current ion sources provide a high ion beam current density ($\sim 1$ mA cm$^{-2}$) at relatively low beam energies (30 – 40 keV).[41, 46] Usually, these sources utilized in industrial ion implanters allow one to create a wide ion beam. High ion beam current density provides implantation depths from a few to tens and even hundreds of nanometres.[4, 24] This is due to accelerated ion diffusion that is stimulated by both rapid defect formation and thermal diffusion. The concentration profiles of implanted ions and elements of the matrix material in the modified layer were calculated[3, 5, 42 – 44, 47 – 49, 59 – 93, 103 – 115] taking into account diffusion, ion mixing and scattering that accompany ion implantation.[76 – 93, 103 – 115] However, no fundamental theoretical description of the distribution of implanted ions with allowance for all processes occurring in the course of implantation is available at the moment. The distribution of ions implanted into the near-surface layer is also significantly influenced by the dynamics of atomic collisions as well as by the accumulation of ion implantation-induced lattice defects.[50, 116 – 132]

The concentration peak of implanted ions $c_{max}$ (see Fig. 1) is usually at a depth of about 20 – 70 nm. Implanted ions collide with atoms of the matrix material; the latter leave their equilibrium positions, thus forming radiation-induced defects. Since the ion energy is a few orders of magnitude higher than the binding energy of atoms in the lattice (about 25 eV for metals), a single implanted ion may displace a total of a few thousands atoms. Thus, ion implantation favours the formation of highly defective regions that are oriented along the ion trajectory, being due to secondary interactions of displaced atoms. This effect is called cascade displacement. Note that usually the concentration profiles of defects and implanted ions are very similar, but the maximum concentration of defects is always at shorter distance to the surface than the maximum concentration of implanted ions.[43, 47, 48]

Implanted ions of light nonmetals (nitrogen, oxygen, *etc.*) are localized in the interstitial space in the crystal lattice of the matrix material. Changes in the properties of surface layers are first of all due to changes in their structure and chemical composition. Owing to nonequilibrium character of the process, ion implantation causes the formation of metastable systems that most often contain nitrides, borides, carbides (depending on the dopant element) or have an amorphous structure. In spite of a large number of possible combinations 'solid – dopant element', a number of characteristic structural phase transformations occurring in solids during ion implantation can be distinguished. Indeed, bombardment of a matrix material by an ion beam leads to changes in its elemental composition in the near-surface layer. Also, ion implantation usually favours fragmentation (reduction of grain size) and homogenization of the structure of a material in the near-surface layers.

Figuratively, the process is a kind of mechanical mixing of materials on the atomic level.[3]

All these transformations in the surface layers from 0.01 to ~1 μm thick lead to formation of regions whose properties are different from those of the matrix material. By varying the type of the dopant elements, the dose, temperature, ion energy and the ion beam current density one can form metastable amorphized near-surface layers.§

## III. Properties of ion-implanted surface layer

Ion implantation significantly influences the mechanical (wear, friction, hardness, fatigue, plasticity, adhesion), chemical (corrosion, oxidation, catalysis) and electromagnetic (electrical conductivity, magnetization, photoconductivity) properties of materials. By appropriately choosing dopant elements and regimes of the process, the method makes it possible to impart desired properties to the surface.

For each dopant element, there exist optimal doses and ion beam energies that allow one to prepare materials with desired properties. Most publications are concerned with ion implantation of nonmetals (nitrogen, carbon, boron, oxygen, argon);¶ studies on ion implantation of metals (titanium, aluminium, copper, molybdenum, tantalum, platinum, tin, *etc.*) are scarce.[44, 45, 49, 50, 95] Current research efforts are mainly focused on implantation of metal ions into alloys, ceramics and polymers to improve their operating properties, such as wear resistance, corrosion resistance and to reduce the friction coefficient.

Ion implantation into structural materials based on titanium and titanium alloys (often utilized as biomaterials) is widely used. The properties of the near-surface layers in titanium alloys change significantly in the presence of alien ions.

### 1. Mechanical and tribological properties

Most publications on ion implantation are devoted to mechanical tests of implanted surfaces because changes in their mechanical properties have complex character. They cannot be explained in detail because a unified theory of hardening of the surface of implanted materials is unavailable at the moment. A number of phenomena [4, 46] are thought to lead to surface hardening upon ion implantation. These are:

— strain hardening;

— breakdown of crystal structure under high implantation doses, *i.e.*, amorphization;

— greater depth of the hardened layer owing to radiation-induced diffusion;

— retardation of dislocations by defects formed in the course of ion implantation;

— changes in the chemical composition of the surface layer;

— formation of solid solutions containing high concentrations of dopant elements that can not be obtained by other doping methods;

— reduction of grain size with simultaneous extension of grain boundaries that slow down or block the motion of dislocations;

— surface plasticization upon implantation of some metal ions (*e.g.*, Sn, Mo) which is due to surface fretting;

— formation of a 'dry lubricant' layer on the surface during implantation of S, Mo + S, N + Ca, O, N + Mo and C ions or formation of surface oxide films that protect the deeper-lying layers from rapid wear.

Key results of ion implantation include an increase in wear resistance that is due to the inceased hardness of the material owing to hardening of the near-surface layer caused by high compressive stress that blocks the motion of dislocations and as a consequence of formation of solid inclusions.

Higher wear resistance of implanted materials is due to reduction of the friction coefficient. Sometimes, in the initial steps of friction, the friction coefficient of implanted layers becomes higher than that of virgin samples and only then decreases. Friction of an implanted material (*e.g.*, steel) is accompanied by micropitting of grains on the surface;[31, 50, 68, 70] this leads to an increase in the working area of friction surface and to healing of cavities formed upon implantation and eventually imparts higher wear resistance to the material. Among various dopant elements (nitrogen, carbon, oxygen, phosphorus, calcium and noble metals), the effect of nitrogen on the changes in the tribological properties has been best studied.[113, 133] Implantation of nitrogen increases the wear resistance of almost all metals. It should be noted that most studies concern implanted alloys based on titanium.

Hardening of nitrogen-implanted titanium alloys is due to various factors, in particular, the formation of a quenched solid solution and to the presence of TiN impurities, grinding of grains in the implanted layer (this in turn causes reduction of the friction coefficient) and the presence of residual stress. The dose of nitrogen ions has the strongest effect on the wear resistance and microhardness of materials. Opinions are different on the nature of the increase in microhardness.[40] A possible reason is defectiveness of the crystal lattice rather than the presence of TiN impurities, namely, the higher the dose of implanted ions the more pronounced crystal lattice breakdown and, as a consequence, the higher the microhardness.

Interpretation of changes in microhardness upon ion implantation is complicated by the fact that in the microhardness tests, the indenter tip often penetrates the material to a depth that exceeds the thickness of the implanted layer. For instance, for implantation of nitrogen into steel ($E$ = 70–100 keV), the modified layer is at most 250–300 nm thick, whereas the indentation depth of a Vickers hardness tester ($H_{V_{0.005}} - H_{V_{0.01}}$) is 0.5–1.5 μm.[5] The values thus obtained characterize the microhardness of the system 'implanted layer/matrix material'.

Note that many studies revealed improvement of the mechanical properties including microhardness of materials at depths that much exceed the penetration depth of implanted ions. This was observed, *e.g.*, after implantation of nitrogen into a steel and titanium alloys and explained [5]

§ Taking into account this fact, some authors (see, *e.g.*, Refs 4, 5, 24) use the term 'ion metallurgy'.

¶ Research on possible industrial applications of implantation with nitrogen, carbon, oxygen and other nonmetal ions in order to improve the mechanical properties of materials has been documented.[17, 20, 39, 44, 49, 50, 61, 64]

by the long-range effect.† More pronounced change in microhardness at such depths can be explained by the effect of radiation-induced diffusion of the dopant element and by the influence of defects created in the crystal lattice in the course of implantation.

In most cases, implantation of metal (Ti, Ta, Mo, Pt) ions into steel also favours an increase in microhardness. This was also observed[5] upon implantation of nitrogen, boron, silicon and carbon ions [$D = (1.2–5) \times 10^{17}$ ion cm$^{-2}$, $E = 70–160$ keV] into steel, the implanted layer being 0.4–0.7 μm thick. A number of studies are devoted to the most important mechanisms that favour improvement of the mechanical properties of steel (in particular, formation in the near-surface modified layer of solid inclusions of nitrides, borides, carbides, *etc.*).[45, 113, 134]

Often, ion implantation causes the formation of 'dry lubricant' in the form of oxide and carbide‡ coatings on the surface of materials; this favours reduction of the friction coefficient and better protection of the surface from wear. Correlations between the mechanical and tribological properties as well as positive effect of ion implantation on these properties have been documented.[38–46]

Changes in the chemical composition of the surface layer may lead to changes in the mechanism of adhesive wear (this can be a reason for reduced expenditure of materials in friction) or to oxidation.[113, 133]

### 2. Chemical properties

Surface modification of metals should not lead to deterioration of their corrosion resistance under operating conditions. The corrosion resistance can be improved as follows:

— by forming a surface layer containing high concentrations (up to 40 at.%) of implanted element (nitrogen, oxygen, *etc.*);

— by implanting ions of the elements suitable for amorphization of the surface layer (calcium, phosphorus, silicon);

— by implanting ions of the elements (platinum, palladium) that induce passivation of metals, *e.g.*, chromium and iron, or change the cathodic reaction kinetics and course of corrosion.

There exist optimal implantation doses of nitrogen ions that impart maximal corrosion resistance to titanium alloys.[44, 135, 136] Depending on the type of the titanium-based alloy and on some other parameters, the implantation dose is varied from $10^{16}$ to $10^{17}$ ion cm$^{-2}$.

Changes in the corrosion resistance of NiTi-based alloys are due to not only structural, but also compositional changes in the modified layer. For instance, depending on the parameters of the process (ion dose, ion energy and ion beam current density) implantation of, *e.g.*, nitrogen may be followed by separation of the ε-$Ti_2N$ and TiN phases dispersed in α-Ti. Implantation of carbon ions results in the formation of TiC. Since the solubility of carbon in α-Ti is lower than that of nitrogen, consumption of TiC with the formation of $TiC_2$ and $Ti_2C$ phases occurs at lower doses. Implantation of oxygen ions leads to formation of TiO or $TiO_2$ depending on dose. Implantation of phosphorus results in the formation of titanium phosphides and to amorphization of the surface.

As mentioned above, changes in the chemical composition and structure of the surface layer cause changes in its mechanical and tribological properties. At high implantation doses ($D \geqslant 10^{18}$ ion cm$^{-2}$), one can form surface layers that are compositionally different from the matrix material. The microstructure and structural phase transformations in the implanted layers have been subjects of numerous studies.[49, 137]

## IV. The shape memory alloys

Considerable literature on shape memory alloys is an indication of interest in unique properties of these systems.[138–141] Studies in this field are aimed at solving technological problems concerning the design of shape memory materials and extension of the field of their application through improvement of properties. Great functional potential of shape memory alloys allows one to solve various materials science, engineering and technological problems; this gave an impetus to discussions on the state of the art in the field, prospects for investigation and application of shape memory materials.[61–64, 72–75, 83–86]

The shape memory effect and superelasticity in NiTi-based alloys have been studied for a few decades.[10–26] Nevertheless, schemes of martensitic transformations in a material are not always readily understandable because these transformations depend on many factors including temperature, mechanical load, crystal lattice deformations, crystallographic parameters, *etc.* Many authors (see, *e.g.*, Refs 138, 141, 142) attempted to explain the effects caused by these factors. In some cases, researchers succeeded to explain dynamic changes observed in studies on deformation in certain samples both experimentally and theoretically.[8, 9, 47, 49, 143–145]

### 1. Mechanisms of the shape memory effect and superelasticity

The shape memory effect and superelastic behaviour of alloys has been known since the 1930s. Systematic studies of martensite structures began in the 1940s.[138] Considerable interest in shape memory materials arose after the discovery of the shape memory effect in NiTi alloy by Buehler *et al.* in 1963.§

† Experimental studies of different properties and microstructure of ion-implanted materials revealed that the effect of ion beams during irradiation of some materials extends to much longer distances as compared to the thin surface layer where retardation of the ions being implanted occurs. These results were first of all obtained for such mechanical properties, as microhardness, wear resistance, friction coefficient, *etc.* Pioneering studies on possible changes in the structural phase state upon ion implantation in deeper-lying layers of the matrix material compared to the thickness of the surface doped layer are now available. There are very few studies on the long-range effect of ion implantation on the structure and properties of semiconductor and metallic materials [see, *e.g.*, A N Didenko, Yu P Sharkeev, E V Kozlov *Metally* (*Metals*), (3), 122 (1993), in Russian]. However, some authors cast doubt on the existence of the long-range effect, because it is not detected in surface studies by nondestructive methods, *e.g.*, positron annihilation, Rutherford backscatttering with channelling and Mössbauer spectroscopy (see, *e.g.*, Ref. 62 and V A Shulov, in *Abstracts of the First International Conference on Ion–Solid Interactions* (Minsk: Byelorussian State University, 1995) p. 26 (in Russian)].

‡ Oxygen and carbon are components of the residual atmosphere in the accelerator chamber.

§ W J Buehler, J Gilfrich, K Wiley. *J. Appl. Phys.* **34** 1465 (1963).

At present, a large number of metallic shape memory systems are known. Among commercially available shape memory systems, nickel alloys (NiTi, NiAl, NiTiFe) and copper alloys (CuZn, CuAlX, CuAlZnX, CuAlFe) are most widely used. Shape memory materials exhibit an unusual behaviour in particular temperature ranges; structural phase transformations occurring in samples under thermomechanical load are now explained. The observed changes are accompanied by complex interplay between the mechanical stress, atomic displacements from equilibrium positions at lattice sites and temperatures in specific ranges. The results of analysis of correlations between thermal and mechanical phenomena as well as the results of materials science studies suggest the possibility of practical application of the shape memory effect in alloys.

**a. The shape memory effect**

Nickel–titanium alloys have different crystal lattices depending on temperature. Below some critical temperature, the lattice is elastic, being characteristic of the martensite phase; above the critical temperature, one deals with a 'rigid' lattice characteristic of the austenite phase. The martensite structure has a lower symmetry compared to austenite. There are various methods to obtain different phases of the martensite structure and only one way to return to the austenite structure. Cooling is accompanied by the formation of several groups of regions with the martensite structure; their deformation causes migration of close-lying boundaries. Eventually, residual deformation of the material ($\varepsilon \neq 0$) may result in the martensite phase with different orientations of the crystal lattice (Fig. 3). Heating of the material in a particular temperature range causes a distorted martensitic transformation to the initial phase (austenite) and subsequent recovery of the initial shape.

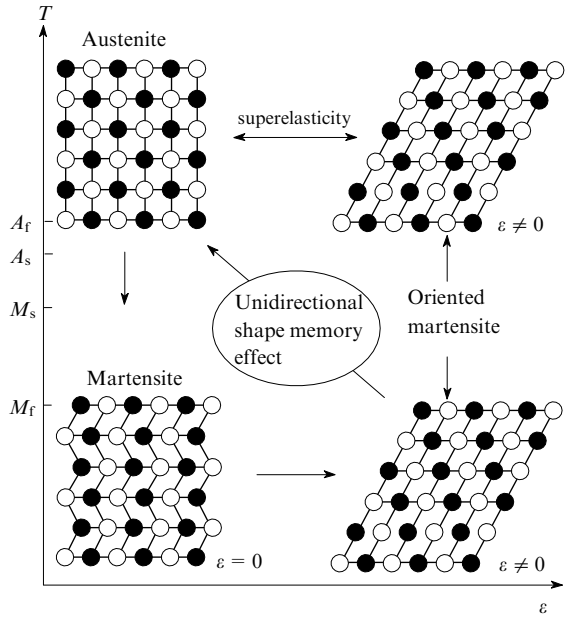



**Fig. 3.** A schematic of phase transformations underlying the superelasticity and shape memory effects.[43]
For the temperatures $A_f$, $A_s$, $M_s$ and $M_f$, see text.

The phenomenon of temperature-induced recovery of the initial shape of a material is called the shape memory effect; it can be uni- and bidirectional. If deformation occurs at ambient temperature, a martensite sample heated in a particular temperature range can recovery its initial shape. This is the unidirectional shape memory effect. The matrix 'remembers' only the shape of the high-temperature phase (see Fig. 3). Heating of deformed samples is accompanied by recovery of the initial shape, whereas no changes in shape occur on cooling. The extent of recovery depends on the deformation degree.

There exist some threshold values of internal stress such that at higher values, the extent of recovery of the initial shape on heating decreases. The reason is that the stress in martensite cannot be higher than the yield stress. Depending on the chemical composition and treatment conditions, the deformation degree of shape memory alloys varies from 4% to 10%.[26] Repeatability of unidirectional shape memory effect on cyclic martensitic transformations is of great practical value. As the number of cycles increases, the extent of shape recovery gradually decreases, whereas for large-amplitude deformations, it is less pronounced. This can be explained by nonideal properties of polycrystalline shape memory materials that show thermoelastic properties at grain boundaries of the matrix phase.

In the case of bidirectional shape memory effect, a material 'remembers' the shapes of both high-temperature and low-temperature phases. The bidirectional shape memory effect is related to cyclic character of phase transformations in a particular temperature range, where reversible changes in shape with no action of external factors are possible. The mechanism of bidirectional shape memory effect is still to be clarified and methods for practical implementation of this effect are of great interest for many researchers.[26]

**b. The superelasticity**

Manifestation of superelasticity by shape memory alloys consists in almost complete recovery of the initial state of the deformed material after unloading provided no changes in external conditions.[25, 141] A stress–strain diagram for the superelasticity effect is shown in the form of the characteristic cycle in Fig. 4. At a stress equal to $\sigma_{a-m}$, the martensite phase is initiated (martensite thermoplasticity); this is the starting point of the martensitic transformation (see below). If the appearance of the martensite phase is induced by thermoelastic stress in the temperature range where the austenite phase is stable, oriented martensite with macroscopic deformation (of the order of a few per cent) is formed.

As a particular critical temperature is reached, a nonlinear elastic deformation (from one to a few per cent) occurs. In the course of unloading, the reverse martensitic transformation begins as the critical point corresponding to $\sigma_{m-a}$ is reached. From this point on, the content of the martensite phase decreases down to complete transformation to the austenite phase. At the instant corresponding to zero stress, a complete (or almost complete) recovery of the initial shape occurs. The stress $\sigma_{m-a}$ necessary to initiate the reverse martensitic transformation is a linear function of temperature provided no constant mechanical stress; therefore, temperature is an important parameter of structural transformations.[26, 138] Martensitic transformations in shape memory materials are characterized by four critical temper-

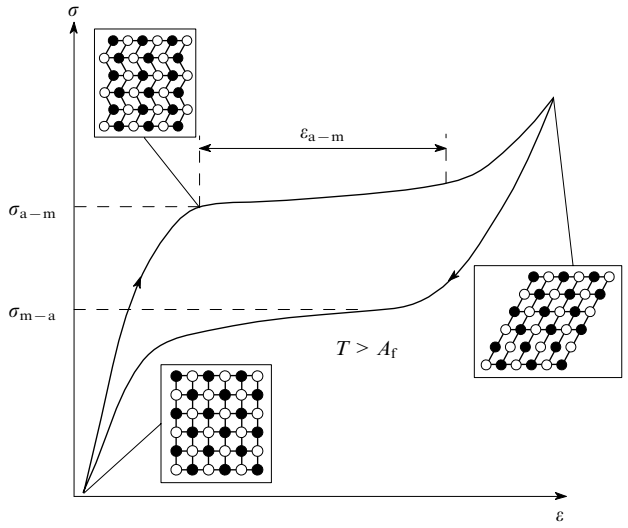



**Fig. 4.** A schematic of the superelasticity effect.[43]

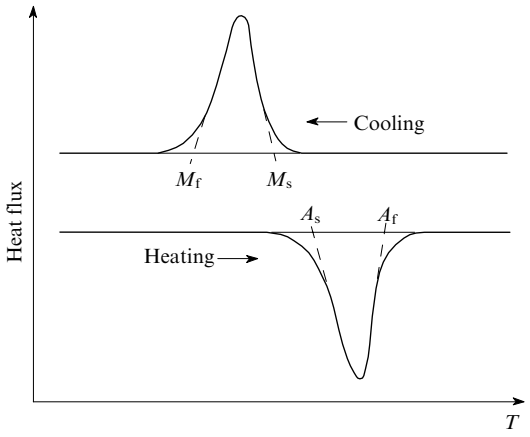



**Fig. 5.** Typical DSC traces for a shape memory material with martensitic phase transitions.[137]

atures $M_s$, $M_f$, $A_s$ and $A_f$ that are usually determined by differential scanning calorimetry (DSC). Figure 5 presents typical DSC traces of a shape memory alloy with clearly seen characteristic temperatures.

At the temperature $M_s$, austenite begins its transformation to martensite on cooling (starting point of the martensitic transformation); $M_f$ is the temperature at which the transformation ceases; $A_s$ and $A_f$ are respectively the temperatures corresponding to the starting point and finish of the reverse transformation from martensite to austenite. The temperatures $M_s$, $M_f$, $A$ and $A_f$ depend on the type of material, specific features of its chemical composition, on the technology and heat treatment of the material.

Physical phenomena underlying the shape memory effect and superelasticity are opposite to the phenomena accompanying thermoelastic martensitic transformations (thermally induced phase transformations in materials). They involve co-operative motion of atoms in the crystal lattice; this can be induced either mechanically (by applying corresponding forces) or thermally (using relevant thermal stresses). Figure 6 presents a constitution diagram of the Ti–Ni system and parameters of the crystal structures of some phases formed in this system. The initiation temperatures of the martensitic transformation is illustrated in Fig. 7. The B2 austenite phase has high lattice symmetry and is stable at higher temperatures. The B19′ martensite phase has a lower lattice symmetry and is stable at lower temperatures (below $M_f$). On cooling below the temperature $M_s$, the B2 phase undergoes transformation to the B19′ phase. This is symbolically represented as B2 → B19′, while the reverse transformation has the form B19′ → B2.

The behaviour of the shape memory alloys in the stress–strain coordinates and correlations between stress as well as the corresponding characteristic temperatures are shown in Fig. 8.

If martensite undergoes self-recovery on unloading, one deals with zero deformation, whereas deformation at temperatures below $M_s$ is due to nonuniformity of the crystal lattice, which manifests itself as macroscopic deformations. Figure 8,*a* presents the stress–strain curves at residual deformation of the material. Heating to a temperature close to $A_s$ induces a martensitic transformation, a deformation martensite transition to the parent phase (austenite) and subsequent recovery of the initial shape.

The reversible thermoelastic martensitic transformation, also called diffusionless transformation, is based on switchable atomic displacements. The term 'diffusionless transformation' means that no long-range diffusion occurs, *i.e.*, atoms do not cross the boundary between the martensite and austenite phases. Switchable character of the transition manifests itself as co-operative atomic displacements caused by transformation of the crystal lattice. Each atom moves unidirectionally and the displacement amplitude is proportional to the distance from the atom to the common plane of the parent phase. This is accompanied by displacements due to shear or twinning, where atoms are displaced as a result of uniform lattice deformation. The overall relative displacement of an atom involved in the martensitic transformation is at most one interactomic distance. As a result, the degree of ordering of atoms and lattice defects, as well as the chemical composition of the martensite phase are the same as those of the austenite phase.

The nature of the shape memory effect and superelasticity are quite understandable; however, theoretical description of the series of phase transitions and their evolution is complicated, still being a subject of intensive experimental and theoretical research.[8, 25, 49, 139, 140, 143, 144]

The mechanisms of the superelasticity and shape memory effects are highly sensitive to external factors, *e.g.*, temperature, stress applied, chemical composition and heat treatment regime. For instance, minor changes (up to 0.1 mass %) in the chemical composition of the most widely used shape memory alloys based on NiTi lead to changes in the characteristic temperatures (up to 10 °C) and, therefore, to changes in the shape of the stress–strain curves ($\sigma-\varepsilon$ plots).

A correct description of the properties in question requires not only knowledge of the chemical composition of the alloy, but also detailed information on all technological operations in each step of treatment of the alloy. Usually, it is difficult to decide which material (in the initial or final step of treatment) should be considered as the base one. Estimation of the Young modulus ($C$) of the NiTi alloy deserves particular attention because its numerical

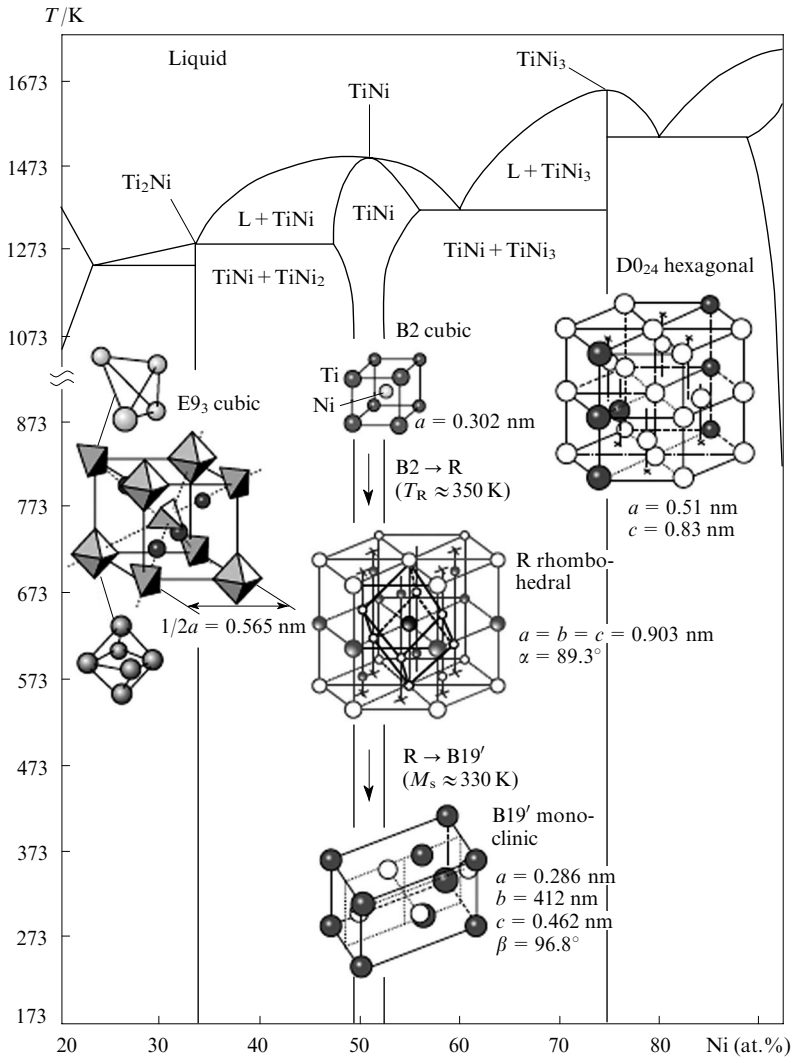



**Fig. 6.** The constitution diagram and crystal structures of some phases in the Ti–Ni system.¶

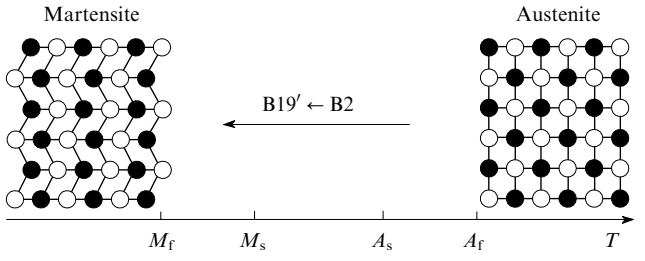



**Fig. 7.** Changes in the characteristic transition temperatures.[43]

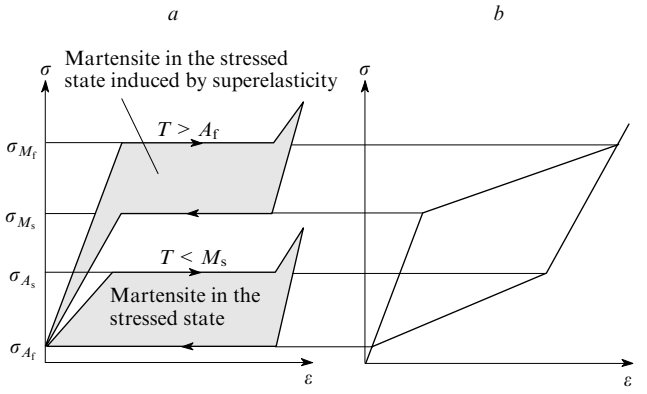



**Fig. 8.** The behavior of the shape memory alloy in the stress–strain coordinates (*a*) and illustration of the relationship between stress and the corresponding characteristic temperatures (*b*).[43]

¶ This diagram appeared in a monograph by V E Günter, V N Khodorenko, Yu F Yasenchuk, T L Chekalkin, V V Ovcharenko, A A Klopotov, G Ts Dambaev, P G Sysoliatin, N G Fomichev, V N Olesova, M Z Mirgasizov, A V Proskurin, R V Ziganshin, V K Polenichkin, A N Matyunin, M Yu Fatyushin, N A Molchanov, A N Monogenov *Titanium Nickelide. A New-Generation Material for Medicine* (Tomsk: Izd. MITs, 2006) (in Russian)]. The book provides a comprehensive description of phases in the Ti–Ni system.

value depends strongly on temperature and can vary from 60 to 70 GPa for the austenite phase as the temperature varies within 15 °C. Thus, parameters of various technological operations performed in the course of treatment of

the shape memory alloys are of great importance for the design of corresponding experiments.

## 2. Mechanical properties of shape memory materials

Shape memory materials have found wide use in medicine (as implants, springs and levers in orthodontics, as surgical and dental tools), mechanical engineering (in production of motors, various types of connectors, temperature sensing elements and actuators) and in production of instruments for seismology.[25] Products from NiTi shape memory alloys were for the first time utilized in 1971; however, the list of application fields of these systems is far from being exhausted.

Yearly, the nomenclature of commercially available products from NiTi alloys extends by 30%. Difficulties in practical application of titanium nickelide are first of all due to its complex thermomechanical behaviour. The high-temperature (parent) austenite phase and the low-temperature martensite phase have different mechanical properties. A typical stress–strain curve of NiTi shape memory alloy (martensite phase) illustrating phase transformations in the system is shown in Fig. 9.

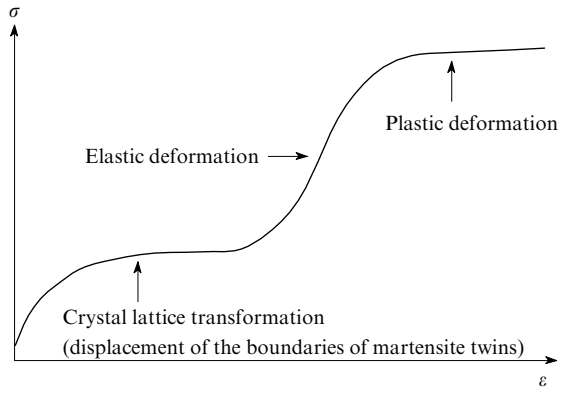



**Fig. 9.** Stress–strain curve of shape memory alloy (martensite phase).[25]

The plot clearly demonstrates three regions, *viz*., the plateau corresponding to the motion of close-lying martensite twins and transformation of the crystal lattice of the martensite phase at the martensite/austenite interface; the region corresponding to elastic deformation of martensite (linear function of strain); and the region corresponding to plastic deformation of martensite.

A comparison of the $\sigma-\varepsilon$ dependences for austenite and martensite revealed different stress values for these phases, which were especially large for NiTi–10%Cu alloys (Fig. 10).

Mechanical properties of shape memory materials are very sensitive to their structure, chemical composition, changes in the temperature of the environment and especially to the phase composition at a given temperature. The temperature dependences of the specific features of deformation processes in shape memory alloys are shown in Fig. 11. As can be seen, cooling of the austenite phase of the material leads to formation of a zero-deformation martensite phase which can exist either in this state or in a mixed (two-phase) state.[138] The martensite phase can be

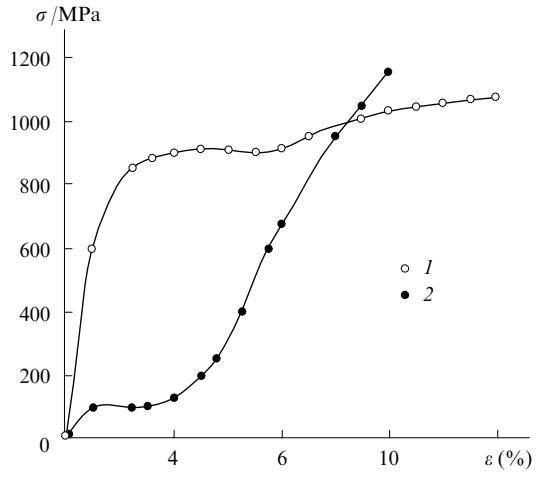



**Fig. 10.** Stress–strain curve of NiTi–10% Cu shape memory alloy in the austenite (*1*) and martensite (*2*) phases.[25]

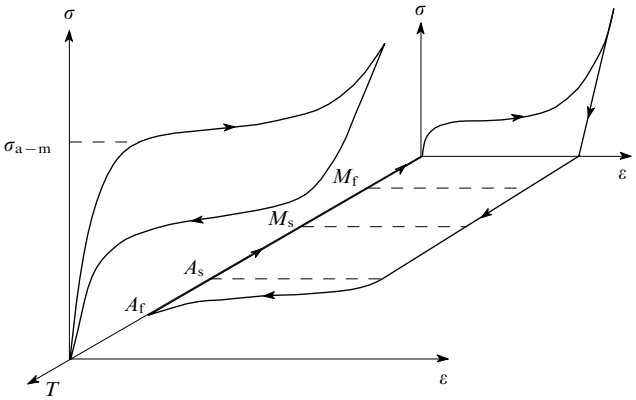



**Fig. 11.** Stress–strain curves of the shape memory alloy at different temperatures.[25]

deformed with ease under relatively low stress. When the 'low-temperature form' of the martensite phase is unloaded, residual deformations are observed. Heating of samples above the temperature $A_f$ causes shape recovery of the 'high-temperature' phase. This is just the case for unidirectional shape memory effect (see above). To keep the material in the austenite phase, the sample is placed in a holder of specified shape and then heated for about 60 min to a temperature much above $A_f$. Often, the so-called learning of the material is used. If the austenite phase is mechanically or thermomechanically loaded at a temperature above $A_f$, the martensitic transformation in the form of superelastic transitions (under cyclic stress) can occur provided that strain is slightly higher than some critical value. Then, the material with the martensite phase exhibits an elastic behaviour. Unloading causes no reverse martensitic transformation, whereas the initial shape is preserved. This process illustrates the phenomenon of superelasticity (see Fig. 4).

As mentioned above, the mechanical and physical properties of shape memory alloys are usually left out of consideration because they depend strongly on the chemical composition and on parameters of technological process

**Table 1**. Properties of shape memory materials.[43]

| Property | NiTi | | Steel | Titanium | Ti–6Al–4V |
|---|---|---|---|---|---|
| | austenite | martensite | | | |
| Microhardness /GPa | 0.10–0.80 | 0.05–0.30 | 0.79–1.20 | 0.390 | 0.83–1.07 |
| Elastic modulus /GPa | 70–110 | 21–69 | 190–200 | 105–110 | 100–110 |
| Ultimate stress /MPa | 1–20 | 700–1000 | 330–600 | 375–540 | 1100 |

and final heat treatment of alloys. That is why the often-cited values of the physical parameters of shape memory materials are guide values (Table 1).

An important advantage of NiTi shape memory alloys over, *e.g.*, systems based on Cu–Zn–Al is the possibility of being treated at higher temperatures (including ion beam treatment) without fear of structure breakdown and disappearance of plasticity. This suggests that the NiTi shape memory alloys are most promising for practical applications.

## V. Influence of ion implantation on the structure of NiTi alloys, the shape memory effect and superelasticity

Among new-generation materials,[25, 145] alloys based on NiTi shape memory alloys are of paramount value for industry,[26, 146] although a correct theoretical model for their behaviour is unavailable. The key problem that precludes wide use of the NiTi alloys consists in the need to modify the surface layer of the material in such a manner that the bulk functional properties, such as the shape memory effect and pseudoelastic deformation, be preserved. Presently, the emphasis in research efforts is placed on the development of methods and technologies for the formation of composite layers with altered properties in the NiTi alloys. In this connection, ion implantation belongs to the most promising technologies.

Most studies on the effect of ion implantation on the surface properties of materials are concerned with titanium and titanium alloys. To improve the tribological properties of titanium alloys, ions of light elements (nitrogen, boron, carbon), inert gases or their combinations are most often used. Note that publications on the formation of surface layers in shape memory materials are scarce. Surface engineering of shape memory materials is a relatively new avenue of research in materials science and usually the results of studies on surface modification are limited in scope or provide one-sided subjective view.[120–126, 129, 134, 136] Numerous publications are devoted to the solution of technological problems related to production of alloys; articles including the description of layer formation on NiTi surface are relatively few. As a rule, many authors restrict their research on fabrication of implanted layers in shape memory materials to studies of the effect of implanted elements on the biocompatibility and corrosion resistance.[138–145]

At the same time, it should be noted that studies of ion-implanted layers not only from the standpoint of their functional properties, but also as subject of basic research are now available. Results of complex investigations of structural-phase changes in materials during ion implantation were reported. Experimental data were obtained by various methods including Auger electron spectroscopy, Rutherford backscattering, X-ray diffraction, grazing-incidence X-ray diffraction, *etc*.

In particular, the effect of ion implantation on the properties of NiTi shape memory alloys under cyclic deformation was studied[147] taking samples of $Ti_{49.8}Ni_{50.2}$ alloy implanted with high doses of $Al^+$ ions as examples. The initial samples were cut as strips $5 \times 30 \times 1$ mm in size and annealed at 673 K. The characteristic temperatures determined by DSC were as follows: $M_f = 279$ K, $M_s = 332$ K, $A_s = 339$ K and $A_f = 363$ K. Two series of $Al^+$-implanted NiTi samples were obtained with the following ion implantation parameters:

series *1*: $D_1 = 1 \times 10^{18}$ ion cm$^{-2}$, $E_1 = 50$ keV;

series *2*: $D_2 = 3 \times 10^{18}$ ion cm$^{-2}$, $E_2 = 150$ keV.

To reveal how ion implantation influences the shape memory effect, stretching tests (shape memory tests) were carried out at $T_1 = 293$ and $T_2 = 373$ K. The authors of Ref. 147 reported the stress–strain curves with indication of the initial and new stress values as well as considered the sequence of phase transformations occurring in the course of tests. Figure 12 presents the stress–strain curves obtained in a single cycle of the shape memory test. The results obtained can be interpreted as follows.

1. Process $0–a$: at $T_1 = 293$ K (for the mixed NiTi structure with higher proportion of martensite with low content of the R-phase), the sample with the martensite structure was deformed by 4% under strain. The $\sigma_m$ value obtained in the first cycle was considered to be the initiation stress for the accommodation of martensite variants or the appearance of the R-phase. The $\sigma_s$ stress was defined as the stress to a 4% strain. The strained sample was in the martensite phase.

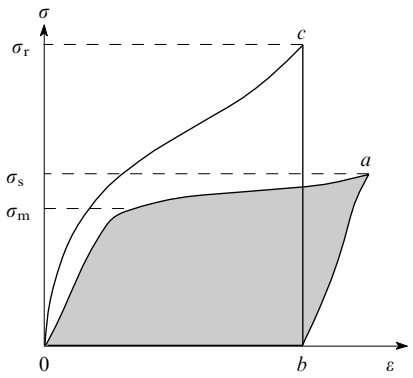



**Fig. 12.** Schematic view of stress–strain curves obtained in a single cycle of shape memory test.[147]

2. Process $a-b$: the sample with the martensite structure was unloaded but remained in the tester; this corresponded to the residual strain state.

3. Process $b-c$: the sample with the martensite structure in the residual strain state was heated to $T_2 = 373$ K corresponding to transformation of the martensite structure to austenite. The internal stress produced by the process ($\sigma_r$) was defined as the shape recovery stress.

4. Process $c-0$: the sample with the austenite structure was unloaded and then cooled to $T_1 = 293$ K and the martensite structure with low content of the R-phase formed again.

The shape memory test curves (Fig. 13) of the NiTi samples clearly demonstrate a significant difference between the implanted and virgin samples. Indeed, an increase in the number of cycles ($N$) leads to changes in the shape of the test curves for both virgin and implanted NiTi alloys. An increase in the number of test cycles causes the stress of formation of the R-phase ($\sigma_m$) to decrease owing to the occurrence of martensitic transformations. The $\sigma_m$ value determined after five cycles of shape memory tests is at most 80 MPa (*cf.* 140 MPa for a single test cycle).

For ion implantation with the dose $D_1$, the stress of formation of the R-phase determined after one test cycle was ~60 MPa (*cf.* about 140 MPa for the virgin material). After five test cycles, the $\sigma_m$ value for the material implanted with the dose $D_1$ is difficult to determine due to the change in the shape of the $\sigma-\varepsilon$ curve. After ion implantation with the dose $D_1$, the $\sigma_s$ value changed as well from about 100 MPa for a single cycle of the shape memory test *vs.* nearly 200 MPa for the virgin material to about 80 MPa after five test cycles. However, the $\sigma_r$ value of the $D_1$-implanted material differed only slightly from that of the unimplanted material, namely, ~200 MPa after single test cycle *vs.* ~190 MPa after five test cycles, respectively. At the higher dose $D_2$, the $\sigma-\varepsilon$ curves differ significantly from the curves typical of the virgin material (see Fig. 13 *c*).

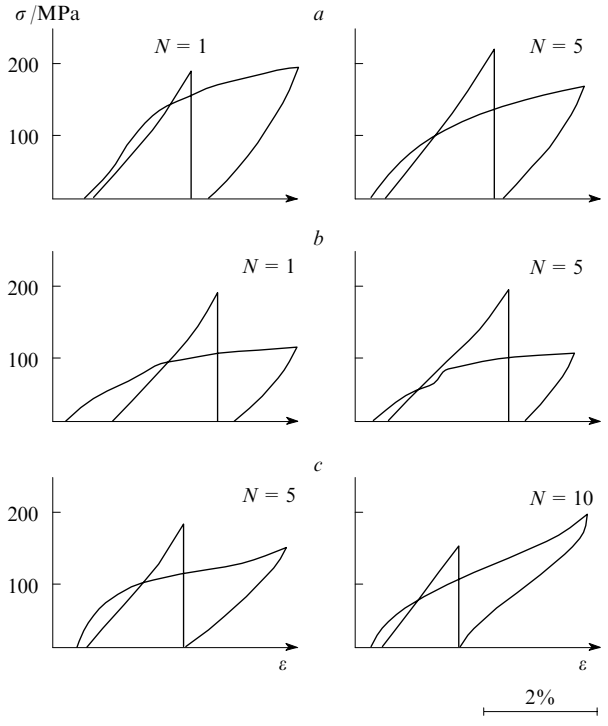



**Fig. 13.** Sample shape memory test curves of NiTi alloy before (*a*) and after implantation with $Al^+$ ions (*b*, *c*).
Ion doses: $D_1 = 1\times10^{18}$ ion cm$^{-2}$ (*b*) and $D_2 = 3\times10^{18}$ ion cm$^{-2}$ (*c*).[147]

Note that after both five and ten cycles of the shape memory test the hardness of the NiTi alloy implanted with the dose $D_2$ increases. The character of the $\sigma-\varepsilon$ curves was explained by simultaneous appearance of the R-phase, austenite and martensite. From Fig. 13 *c* it follows that the $\sigma_m$ value is difficult to determine because the curves show no plateau characteristic of the shape memory alloy. After ten cycles of the shape memory test, the $\sigma-\varepsilon$ curve is steeper than after five test cycles and differs appreciably from the corresponding curves for the virgin and $D_1$-implanted materials. The $\sigma_s$ and $\sigma_r$ values also changed after implantation with the dose $D_2$, being equal to 140 and 180 MPa, respectively, after test cycles. If at the dose $D_1$, the recovery stress $\sigma_r$ hardly changed, it decreased at the higher dose $D_2$. It is believed[147] that changes in the $\sigma_m$, $\sigma_s$ and $\sigma_r$ parameters are due to significant structural distortion and changes in the chemical composition of the implanted regions in the surface layer that occur at the high implantation dose ($D_2 = 3\times10^{18}$ ion cm$^{-2}$). Implantation with the high ion dose leads to considerable changes in realization of the shape memory effect. The results obtained by Rutherford backscattering and X-ray diffraction analysis showed that the ion-modified layer is 0.5–0.6 μm thick under these doses.

Changes in the structure and mechanical properties of $Ni_{46}Ti_{54}$ alloy after implantation of nitrogen and boron ions were analyzed.[148] Austenite samples 20 mm long were cut from a NiTi wire 1.5 mm in diameter, ground and polished with diamond pastes (9, 3, 1 μm).† The implantation dose and energy were the same for the boron and nitrogen ions, *viz.*, $D_1 = 10^{16}$, $D_2 = 5\times10^{16}$, $D_3 = 1\times10^{17}$ ion cm$^{-2}$; $E = 150$ keV. It was shown that at all implantation doses, the surface roughness remained unchanged; however, no roughness value was reported. Changes in the phase composition and microstructure were determined by grazing incidence X-ray diffraction that enables studies at depths from 0.56 to 2.8 μm depending on the angle of incidence of X-ray radiation. Surface sublayers enriched with titanium oxides, borides and nitrides were found. The implanted layer was 0.35 μm thick for implantation with nitrogen and 0.4 μm thick for implantation with boron. It was shown that the microstructure and phase composition of the implanted layers are dose-dependent, namely, the surface layer of austenite implanted with nitrogen ions contained the B2 phase at all doses, but the content of this phase was different for different doses. For low doses ($10^{16}$ ion cm$^{-2}$), the X-ray diffraction patterns exhibit a peak corresponding to the martensite phase B19′. An increase in the implantation dose to $5\times10^{16}$ ion cm$^{-2}$ led to domination of the base phase, whereas at the high dose ($10^{17}$ ion cm$^{-2}$), the surface layer contained both martensite and austenite phases.

The mechanical properties of the surface NiTi alloys were improved by various methods.[149] To attain amorphization of the surface, defects were introduced into the

† Numbers in parentheses denote the grain size of the major fractions.

crystal lattice in two ways, by mechanical treatment of the surface (shot-peening) and by implantation with nitrogen ions. Two series of NiTi samples were used, austenite $Ni_{48.9}Ti_{51.1}$ (series *1*) and martensite $Ni_{50.9}Ti_{49.1}$ (series *2*). The $A_f$ temperature was 314 K for the first and 329 K for the second series. After implantation, these characteristic temperatures were unchanged. The values of other characteristic temperatures were not reported. Disk-shaped samples 3 mm in diameter were annealed at 873 K for 30 min and polished with diamond pastes (6 and 1 μm). Shot-peening (diameter of glassy media varied from 50 to 300 μm) was carried out under controlled pressure and peening duration. Under shot-peening hardening of the surface, samples were located at a fixed distance from the outlet. Implantation of nitrogen ions ($E = 100$ keV) was performed in different doses from $2 \times 10^{12}$ to $10^{18}$ ion cm$^{-2}$. Based on the results of microhardness measurements using a Knoop test with a load of 10 g, the microhardness of the modified surface was plotted *vs.* load and implantation dose. The microhardness of the samples under study (for both martensite and austenite phases) was $150\,N_{KN\,10g}$ (1.5 GPa). The microhardness of the work-hardened surface gradually increased with the load and reached a value of $500\,N_{KN\,10g}$ (5 GPa) at a pressure of $7 \times 10^5$ Pa (this corresponded to a treatment duration of 60 s). The microhardness of the implanted surface varied from $200\,N_{KN\,10g}$ (2 GPa) at a dose of $5 \times 10^{16}$ ion cm$^{-2}$ to $350\,N_{KN\,10g}$ (3.5 GPa) at a dose of $2 \times 10^{17}$ ion cm$^{-2}$ for the austenite samples and from $180\,N_{KN\,10g}$ (1.8 GPa) at a dose of $5 \times 10^{16}$ ion cm$^{-2}$ to $270\,N_{KN\,10g}$ (2.7 GPa) at a dose of $2 \times 10^{17}$ ion cm$^{-2}$ for the martensite samples.

A transmission electron microscopy (TEM) study of amorphized surfaces of the implanted and mechanically treated martensite and austenite samples revealed the formation of regions with high density of dislocations in the modified layer at pressures of $6 \times 10^5$ and $7 \times 10^5$ Pa for shot-peening and at a dose of $2 \times 10^{16}$ ion cm$^{-2}$ for ion implantation. This indicates large plastic deformations induced by mechanical treatment, especially in the ground (finely dispersed) regions. Other published data indicate that the surface of NiTi alloys can be amorphized with ease using various treatment procedures including ion mixing, mechanical melting and ion implantation. Amorphization occurs as a result of introduction of defects into the crystal lattice of the material. Therefore, in the mechanically treated samples the regions with the highest degree of amorphization are better seen in the TEM images. In the case of ion implantation, the concentration of radiation-induced defects abruptly increases as the ion dose increases from $2 \times 10^{16}$ to $10^{18}$ ion cm$^{-2}$. The conclusions drawn [149] are as follows: (i) modification of the surface of NiTi alloys by shot-peening hardening and ion implantation leads to an increase in the surface hardness and a decrease in the friction coefficient and (ii) these treatment procedures do not influence the temperatures of the modified layer and allow one to improve the surface properties of the alloys without deterioration of their functional properties.

No concentration profiles of the surface layer were reported,[149] although TEM allows these studies to be carried out. These data would be of importance to establish correlations between the properties of the composite system 'modified layer/matrix material', type and surface treatment parameters.

Among the studies on implanted NiTi alloys (austenite phase), there are Refs 148 and 150. It was concluded [148] that the implanted nitrogen layer 0.3 μm thick contains almost equal amounts of the B2 and B19′ phases. At all doses of implanted boron and nitrogen ions, the modified layer contained the B2 phase. But unlike implantation of nitrogen, at the same dose of implanted boron ions ($10^{16}$ ion cm$^{-2}$), the surface layer mainly contained the B19′ phase, which was not detected after implantation of high ion dose ($10^{17}$ ion cm$^{-2}$).

An attempt to elucidate the effect of double implantation of $Cu^+$ (dose $0.7 \times 10^{17}$, $1.4 \times 10^{17}$, $2.1 \times 10^{17}$ ion cm$^{-2}$) and $Ti^+$ ions ($10^{17}$ ion cm$^{-2}$) on the mechanical properties and shape memory effect in NiTi alloys was reported.[151] The phase composition was analyzed using $Ni_{49.5}Ti_{50.5}$ samples $1 \times 15 \times 15$ mm in size, while mechanical tests were performed with samples $1 \times 1 \times 40$ mm in size. The samples were preliminarily annealed in a vacuum furnace at 1073 K for 1 h, their surfaces were electrochemically etched in a solution of acetic acid and 10% $HClO_4$. Powder X-ray diffraction revealed the presence of the B2 phase (97%) and the $Ti_2Ni$ secondary phase (3%). The characteristic temperatures were as follows: $M_s = 283$, $M_f = 261$, $A_s = 299$ and $A_f = 322$ K. The test of the mechanical properties of $Ni_{49.5}Ti_{50.5}$ samples included loading under constant torque moment at a temperature above $A_f$ followed by cooling in the stressed state to a temperature below $M_f$, unloading and heating again to a temperature above $A_f$. The torsion angle was measured after loading ($\gamma_{total}$) and unloading ($\gamma_{B2-B19'}$). The $\gamma_{total}$ and $\gamma_{B2-B19'}$ values were reported as parameters of the shape memory effect. Experiments revealed improved parameters of deformation, namely, the angles $\gamma_{total}$ and $\gamma_{B2-B19'}$ in the implanted samples appeared to be larger than in the virgin samples; this was explained by greater degree of reorientation of martensite in the implanted material under stress. It is believed [151] that under thin implanted layer there is a layer characterized by higher internal stress that favours reorientation of martensite. Also, the martensitic transformation temperatures change upon implantation of $Cu^+$ and $Ti^+$ ions; this influences the changes in the characteristic temperatures of phase transformations under different loads. For instance, unimplanted and $Cu^+$-implanted (dose is $2.1 \times 10^{17}$ ion cm$^{-2}$) samples are characterized by $\Delta T = 32$ K and 15 K, respectively, at 100 MPa.

It was concluded that in the case of double ion implantation the properties of NiTi alloys are influenced by not only the chemical and phase compositions and the structure of the implanted layer, but also by the microstructure of deeper-lying layers. According to Auger electron spectroscopy data, the thickness of the modified layer is ~200 nm after double implantation. No nickel was detected at depths <25 nm. At depths in the range 30–40 nm, a very low content of nickel was detected; at a depth of 50 nm, $TiO_2$ was the major phase. Tensile tests of $Ni_{49.5}Ti_{50.5}$ alloy were carried out at room temperature. An analysis of the $\sigma-\varepsilon$ curves showed that the hardness of the implanted sample was lower than that of the virgin sample. For instance, the stress at 8% strain was 600 MPa for the virgin and 500 MPa for the implanted material. Implanted samples were characterized by larger plastic deformation compared to the unimplanted ones.

The physical properties of the modified surface layers of a NiTi alloy were analyzed to assess the potential for

biomedical applications.[152] The goal of that work was to study the behaviour of the modified layers at different degrees of surface wetting. The surfaces of samples of the austenite ($A_f = 298$ K, $Ni_{51.1}Ti_{48.9}$) and martensite ($A_f = 351$ K, $Ni_{48.2}Ti_{51.8}$) phases of NiTi alloy were independently modified by implantation with nitrogen ions ($D = 2 \times 10^{17}$ ion cm$^{-2}$, $E = 100$ keV) and by shot-peening (as in Ref. 149, the diameter of glassy balls also varied from 50 to 300 μm). Using X-ray photoelectron spectroscopy, it was shown that the alloy treated by both methods contains $TiO_2$, TiN as well as calcium, silicon and sodium compounds. The content of nickel in the modified layer also remained unchanged for both kinds of treatment. The authors of Ref. 152 believed that changes in the chemical composition of the modified surface will not suppress the shape memory effect in the material, although experimental studies of relevant conditions were not reported.

It was assumed that, in spite of the presence of the amorphized layer that formed on the surface of NiTi samples after implantation and shot-peening, the presence of titania proves their biocompatibility. The degree of wetting of the NiTi surface with distilled water was estimated by measuring the contact angle between the surface and a liquid drop at room temperature. It was found that for both surface modification techniques, the austenite samples are characterized by larger contact angles than the martensite samples. It was concluded that the wettability of surface-modified NiTi alloy allows one to use it as biomaterial.

In discussing the influence of ion implantation on the shape memory effect and corrosion resistance of NiTi alloy the emphasis was placed on changes in the phase composition and microstructure of implanted layers. The implantation parameters of nitrogen ions were calculated using the TRIM'91 software. The estimated average projected ranges of nitrogen ions implanted into the NiTi samples are listed in Table 2.

**Table 2**. Estimated projected range of nitrogen ions implanted into NiTi samples.[152]

| $D$ /ion cm$^{-2}$ | $E$ /keV | $l$ /μm |
|---|---|---|
| $5 \times 10^{17}$ | 50 | 0.063 |
| $5 \times 10^{17}$ | 100 | 0.123 |
| $10^{17}$ | 50 | 0.063 |
| $10^{17}$ | 100 | 0.123 |
| $10^{16}$ | 50 | 0.063 |
| $10^{16}$ | 100 | 0.123 |
| $10^{15}$ | 100 | 0.123 |
| $10^{15}$ | 250 | 0.280 |

A NiTi layer about 500 nm thick implanted individually with nitrogen ions ($D = 5 \times 10^{17}$ ion cm$^{-2}$), argon ions ($D = 3 \times 10^{17}$ ion cm$^{-2}$), as well as exposed to double ion implantation with $Ar^+ + N^+$ was studied.[60] The modified layer contained ~40 at.% of nitrogen within 55 nm from the surface in the first case and 35 at.% of nitrogen within 75 nm from the surface after double ion implantation. Such a treatment led to significant changes in the elemental depth distribution within the surface layer, and the so-called sublayer enriched with the substrate constituent elements (enriched buried layer) was formed. The $N^+$-implanted surface layer contained no nickel at depths 50 – 70 nm.

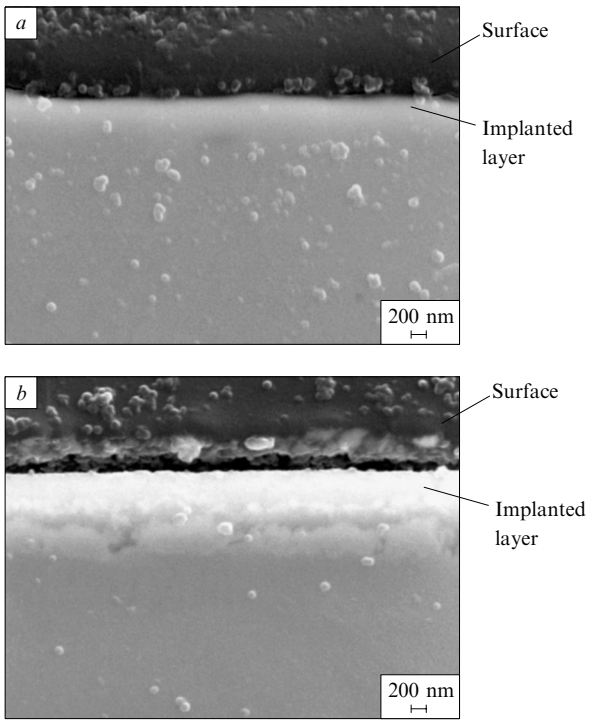



**Fig. 14.** SEM images of NiTi samples (martensite phase) implanted with nitrogen ions at different implantation parameters.[133]
(*a*) $D_1 = 2 \times 10^{17}$ ion cm$^{-2}$, $E_1 = 60$ keV;
(*b*) $D_2 = 2 \times 10^{18}$ ion cm$^{-2}$, $E_2 = 65$ keV.

Nitrogen was detected at depths from 80 to 100 (and even 500) nm. It was shown that double implantation with $N^+ + Ar^+$ ions favours the formation of Ti – N – O systems at a depth of 70 nm from the surface.

The thickness of the layer implanted with different doses of nitrogen ions was evaluated using NiTi samples (martensite, series *1*)[133] using a scanning electron microscope (SEM) operating in the secondary-electron mode. The SEM images (Fig. 14) showed that ion implantation first of all causes a change in the colour of the layer, thus indicating certain changes in its chemical composition. The chemical composition was not analyzed because the microscope was not equipped with energy-dispersive detector. Gradual change of the colour from light (top) to dark (bottom) is characteristic of implanted layers and indicates the lack of well-defined interface between the ion-modified surface layer and the matrix material. The thickness of the modified layer was estimated as ranging from 270 to 350 nm.

The elemental depth distribution was estimated[128] by analyzing the Rutherford backscattering spectra using original models and software (see Ref. 153). The results obtained are presented in Fig. 15. After implantation of nitrogen ions into the surface of NiTi samples ($D = 10^{18}$ ion cm$^{-2}$, $E = 60$ keV) the nitrogen concentration equal to 41 at.% at a depth of 50 nm gradually decreases with depth and approaches zero at a depth of 225 nm. Simultaneously, a low concentration of nickel is detected at a depth of about 50 nm. As the distance from the surface increases, the content of nickel gradually increases, reaches a maximum value (59 at.% – 60 at.%) at

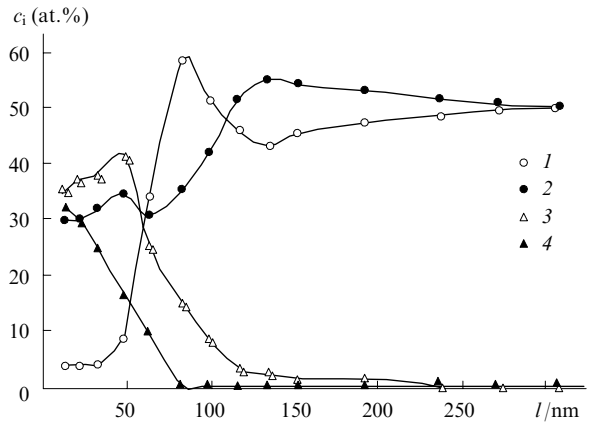



**Fig. 15.** Concentration profiles of elements in the surface layer of NiTi alloy (martensite phase) implanted with nitrogen ions ($D = 10^{18}$ ion cm$^{-2}$, $E = 60$ keV) obtained from Rutherford backscattering spectra.[128]
Element: Ni (*1*), Ti (*2*), N (*3*) and O (*4*).

depths 75–100 nm and then decreases to a value of nearly 50 at.% which is characteristic of the matrix material. The concentration of titanium also changes from 30 at.% near the surface to 52 at.% at a depth of about 150 nm.

Thus, implantation of nitrogen ions (as well as boron and other elements) leads to sputtering of some nickel and titanium atoms from the surface layer of NiTi alloy, whereas other atoms move into the interior of the material, as indicated by the results of analysis of the Rutherford backscattering spectra. Mention may be made that the sputtering rate of nickel atoms in the course of implantation was noticeably higher than that of titanium atoms.

Crystallographic data for the structures determined after crystallization of the phases found in the NiTi alloy implanted with a high dose of nitrogen ions are listed in Table 3 and presented in Fig. 16.

Processing of diffraction patterns showed that a decrease in the layer thickness to ~170 nm is accompanied by a decrease in the intensities of the martensite peaks, whereas the intensities of the peaks corresponding to other phases did not change. An analysis of all diffraction patterns revealed a common feature, *viz*., a change in the phase composition of the alloy with a decrease in the effective thickness of the layer in question. The diffraction patterns exhibit lower intensities, small shifts and broadening of the diffraction lines in the vicinity of the martensite phase $M_m$, and a simultaneous increase in the relative intensity of the diffraction lines of the phases $M_v$, $Ni_4Ti_3$ and TiN. The depth distribution of the phases is as follows: no $M_m$ martensite phase was detected within the layer ~340 nm thick and the $M_v$ phase was detected within the ~170 nm thick layer. Also, all diffraction peaks appeared to be shifted which indicates some lattice distortion. As the effective layer thickness decreases, the diffraction patterns exhibit changes in the phase composition of the alloy, namely, weakening as well as small shifts and broadening of the diffraction lines of the $M_m$ phase and an increase in the relative intensities of the diffraction lines of the $M_v$, $Ni_4Ti_3$ and TiN phases.

At a layer thickness of about 340 nm, the martensite phase is no longer detected (there are no lines from this phase in the diffraction pattern, see Fig. 16 *e*). Further decrease in the effective layer thickness to ~170 nm causes a small decrease in the intensities of the diffraction lines from the $M_v$ phase. The observed shift of the diffraction line indicates a lattice distortion.

Using secondary-ion mass spectrometry (SIMS), one can analyze the molecular and elemental compositions of layers as well as the elemental depth distributions. This is a destructive method of investigation because the sample surface is sputtered (so-called ion etching of the sample surface). Usually, it is used to determine the content of particular components in the course of successive removal (etching) of atomic layers. In particular, SIMS was used to assess the projected range of nitrogen ions depending on the implantation parameters.[43, 150, 153, 154] The concentration (ion cm$^{-3}$) profiles of the martensite and austenite phases of NiTi alloy implanted with nitrogen and base elements were reported.[43]

To compare the implantation depths for the martensite and austenite phases, a commercially available titanium alloy implanted with nitrogen ($D = 10^{18}$ ion cm$^{-2}$, $E = 60$ keV) was additionally studied. Martensite samples (series *1*) used in the SIMS studies were implanted with different doses of nitrogen ions:

— series *1*: $D = 10^{16}$, $10^{17}$, $10^{18}$ and $5 \times 10^{18}$ ion cm$^{-2}$, $E = 55$ keV;

— series *2*: $D = 10^{17}$, $5 \times 10^{17}$ and $1.5 \times 10^{18}$ ion cm$^{-2}$, $E = 55$ keV.

An analysis of the SIMS profiles obtained for the samples of series *1* at different implantation doses (see Fig. 17) suggests that at $D = 10^{16}$ ion cm$^{-2}$, the concentration of nitrogen atoms in the layer is lower than at higher doses. The concentration profiles of nitrogen ions clearly showed a decrease in their content with respect to the depth. At a dose of $10^{16}$ ion cm$^{-2}$, the thickness of the nitrogen-rich layer is ~0.11–0.12 μm (see Fig. 17 *a*). As the dose increases to $10^{17}$ ion cm$^{-2}$ (see Fig. 17 *b*), the implantation depth increases, the maximal concentration of nitrogen is

**Table 3**. Parameters of structures found in phases of nitrogen-implanted NiTi alloy ($D = 10^{18}$ ion cm$^{-2}$, $E = 50$ keV).

| Phase | Structural type | Lattice | Space group | Lattice constants | | | | |
|---|---|---|---|---|---|---|---|---|
| | | | | $a$/nm | $b$/nm | $c$/nm | $\beta$/deg | $\gamma$/deg |
| Austenite | NiTi | cubic | *Pm*3*m* (221) | 0.3012 | – | – | – | – |
| Martensite, $M_m$ | NiTi | monoclinic | $P2_1/m$ (11) | 0.4622 | 0.4120 | 0.2885 | 96.8 | – |
| Martensite, $M_v$ | NiTi | " | $P2_1/m$ (11) | 0.2898 | 0.4108 | 0.50789 | 97.78 | – |
| $Ni_4Ti_3$ | $Ni_4Ti_3$ | rhombohedral | *R*3*m* (148) | 1.1235 | – | 0.4646 | – | 120 |
| TiN | TiN | cubic | *Fm*3*m* (225) | 0.424 | – | – | – | – |

**Note**. Shown are the data taken from the Powder Diffraction File (http://www.icdd.com/translation/rus/pdf4.htm).

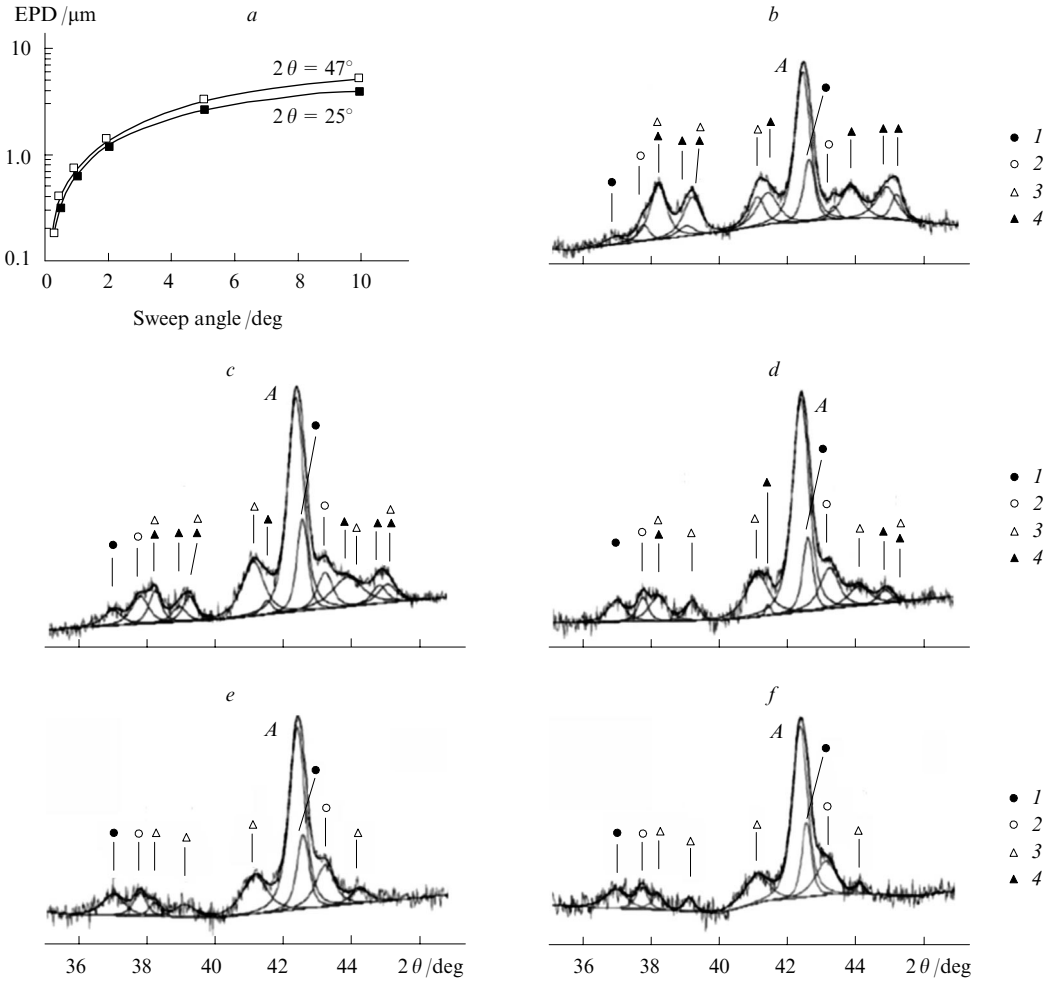



**Fig. 16.** Effective penetration depth (EPD) of X-ray radiation plotted *vs.* angle of incidence of the ion beam (*a*) and the X-ray diffraction patterns of implanted NiTi alloy ($D = 10^{18}$ ion cm$^{-2}$, $E = 50$ keV) obtained at fixed angles of incidence of CuK$_\alpha$ radiation (*b*–*f*); peak *A* corresponds to the austenite phase.[150]
(*1*) NiTi, (*2*) $Ni_4Ti_3$, (*3*) $M_v$, (*4*) $M_m$.

| Position | *b* | *c* | *d* | *e* | *f* |
|---|---|---|---|---|---|
| Angle of incidence /deg | 5 | 2 | 1 | 0.5 | 0.25 |
| EPD /μm | 3 | 1.3 | 0.67 | 0.34 | 0.17 |

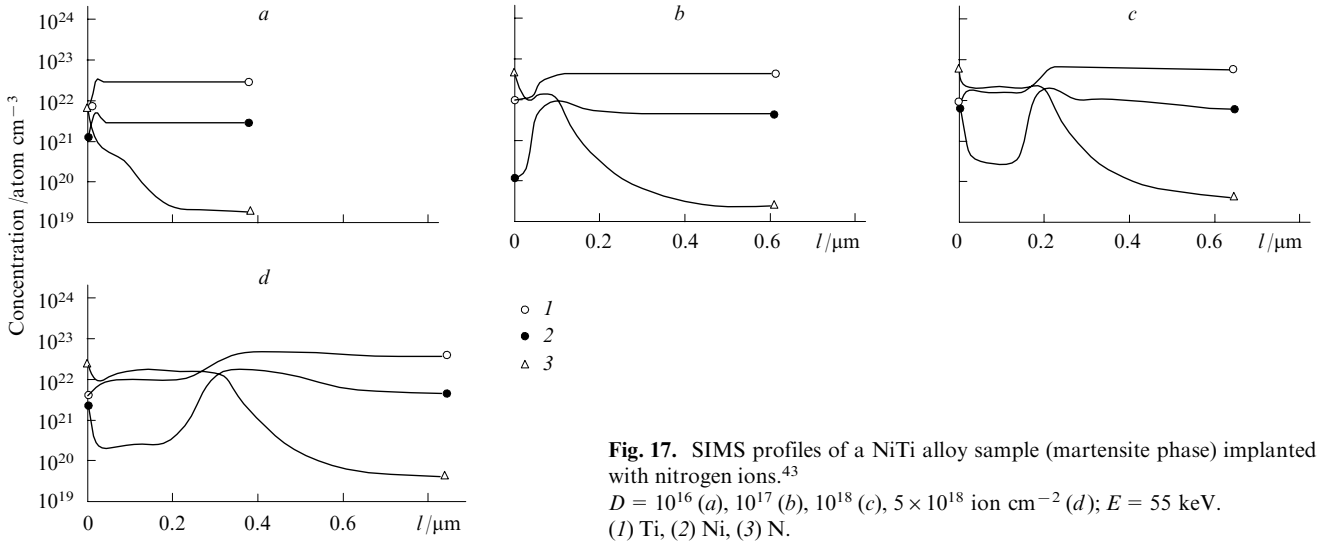



**Fig. 17.** SIMS profiles of a NiTi alloy sample (martensite phase) implanted with nitrogen ions.[43]
$D = 10^{16}$ (*a*), $10^{17}$ (*b*), $10^{18}$ (*c*), $5 \times 10^{18}$ ion cm$^{-2}$ (*d*); $E = 55$ keV.
(*1*) Ti, (*2*) Ni, (*3*) N.

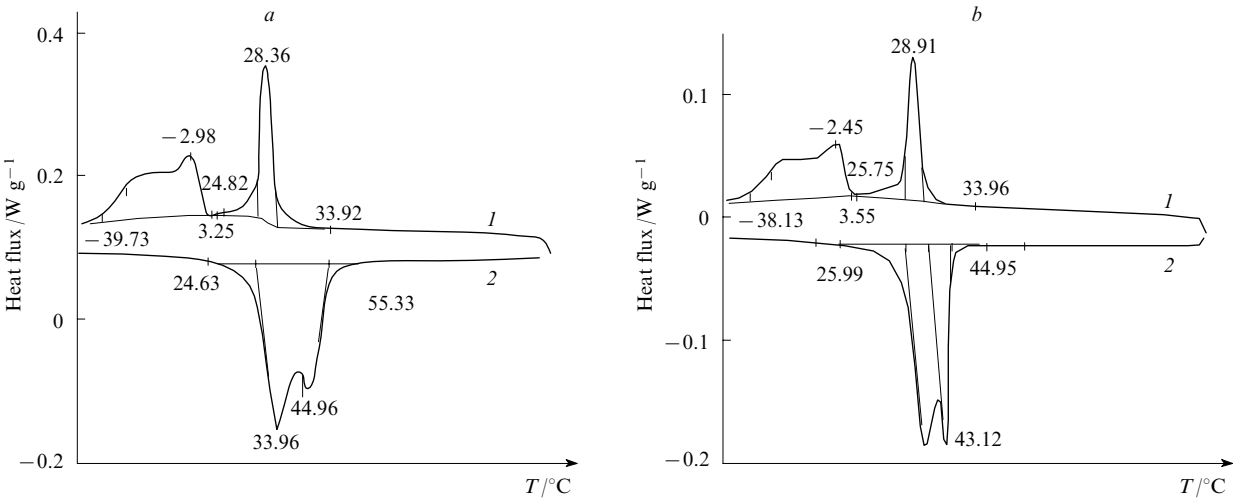



**Fig. 18.** DSC traces of NiTi alloy (martensite phase) implanted with nitrogen ions ($D = 10^{18}$ ion cm$^{-2}$, $E = 55$ keV): one (*a*) and two (*b*) cooling–heating cycles.[34]
Cooling (*1*), heating (*2*); numbers near DSC traces: temperatures /°C.

determined at a depth of 0.05 μm, while the thickness of the implanted layer is ~0.25 μm. At high implantation doses ($10^{18}$ and $5 \times 10^{18}$ ion cm$^{-2}$), the SIMS profile of nitrogen is broadened, a characteristic plateau appears (see Fig. 17 *c*,*d*) and the thickness of the implanted layer also increases to ~0.38 and ~0.45 μm, respectively.

Implantation of nitrogen ions ($D = 10^{18}$ ion cm$^{-2}$, $E = 55$ keV) causes changes in the characteristic of temperatures of the martensite phase of NiTi alloy. The DSC traces for implanted samples of NiTi are shown in Fig. 18.

Nitrogen-implanted NiTi alloy is a mixture of the R-phase and martensite; however, the temperature corresponding to the appearance of this mixture was much higher than for the virgin sample and varied from ~ −40 to 35 °C; The characteristic starting and final transition temperatures were as follows: $R_s = 33.92$, $R_f = 24.82$, $M_s = 3.25$ and $M_f = -39.73$ °C).

The temperature range for the first heating cycle for the implanted samples is much wider than for the unimplanted samples, $A_s = 24.53$ °C *vs.* $A_f = 55.33$ °C, respectively. Then, the characteristic temperatures of the cooling–heating cycles somewhat change compared to those for the first cycle. However, on subsequent heating the thermal peak is narrower than for the first cycle. The sequence of phase transformations on cooling remains unchanged. The transition temperatures for second cooling–heating cycle of the implanted NiTi alloy are $R_s = 33.96$, $R_f = 25.75$, $M_s = 3.55$, $M_f = -38.13$, $A_s = 25.99$ and $A_f = 44.95$ °C.

## VI. Influence of high doses of implanted ions on physicomechanical properties of NiTi alloys

As mentioned above, NiTi shape memory alloys are of considerable interest for various practical applications. In particular, this is indicated by publication of numerous studies on improvement of the mechanical and physicochemical properties of the surface layers of shape memory materials with preservation of their functional properties.

For instance, the results of studies on the mechanical properties of NiTi samples of different chemical compositions are available.[6,155] Two series of samples were studied, $Ni_{50.8}Ti_{49.2}$ (series *1*, martensite) and $Ni_{49.0}Ti_{51.0}$ (series *2*, austenite).[6] Crystallization and shape 'imprinting' were attained by annealing the samples at 773 K. Both series of thin-film samples fabricated by magnetron sputtering represented 6.5 (series *1*) and 6 μm (series *2*) thick disks. The transition temperatures (°C) determined by DSC were as follows:

for samples from series *1*: $M_s = 65$, $M_f = 60$, $A_s = 87$, $A_f = 95$;

for samples from series *2*: $M_s = -38$, $M_f = -59$, $A_s = 3$, $A_f = 97$.

After ion implantation, both series of samples appeared to be wear resistant and to have a reduced value of the friction coefficient compared to the virgin samples.

The authors of Ref. 6 reported the results of the nanoindentation and membrane tests. Detailed information on these experiments is unavailable. The results of the indentation tests (calculated with respect to a depth range from 30 to 1000 nm) of the martensite samples showed that the Young modulus ($C$) gradually decreases from 45–50 GPa ($h = 80$–$100$ nm) to 20–15 GPa ($h = 500$ nm) as the indenter penetration depth ($h$) increases. A single point on the stress–strain curve corresponds to fifteen same-type measurements. Further increase in the indenter penetration depth ($h \approx 1000$ nm) led to the Young modulus values that were close to those obtained from the results of the membrane test (~12–15 GPa).

An analysis of the dependence of the Young modulus on the indentation depth obtained for the austenite samples at room temperature suggests a phase transition A → M at the indentation points. At small indenter penetration depths (10–100 nm), the Young modulus is 110 GPa, being close to the value determined from the membrane test. As for the martensite samples, the Young modulus decreases to 20 GPa as the indenter penetration depth increases.

It was reported that the microhardness of the material ($H$) also decreases as the indenter penetration depth increases. Indeed, one gets a decrease in the microhardness from 14 GPa ($h = 80$–$100$ nm) to 4 GPa ($h = 700$–$800$ nm) for the martensite samples and from 1.2–1.3 GPa ($h = 100$ nm) to 0.1–0.6 GPa ($h = 700$–$900$ nm) for the

austenite samples. The possibility for high stress to develop around the indenter tip and some replication of the martensitic transformation A → M (also for the austenite samples) were suggested. The Young modulus of austenite gradually decreases as the indenter penetration depth increases. The authors of that study believe that this decrease is related to the development of a locally possible martensitic transformation in austenite. The Young modulus of NiTi (martensite) also decreases as the indenter penetration depth increases. It was assumed that local stress of the material may lead to transformation of the local martensite regions and to reorientation of martensite or local formation of a new martensite region.

The surface of $Ni_{50}Ti_{40}Zr_{10}$ alloy was implanted with molybdenum ions ($D_1 = 1.8 \times 10^{17}$ and $D_2 = 5 \times 10^{17}$ ion cm$^{-2}$, $E = 50$ keV).[156] That work mainly concerned (i) structural changes in $Ni_{50}Ti_{40}Zr_{10}$ at different depths and (ii) surface characterization under different loads of the material. Needle-shaped ($1 \times 1 \times 20$ mm) and plate-like ($1 \times 10 \times 20$ mm) $Ni_{50}Ti_{40}Zr_{10}$ samples were polished in a hot solution comprising 89 ml $H_2O$ + 2 ml HF + 2 ml $HNO_3$. It was found that the martensitic transformation in the material obeyed the simple scheme B2 ⇄ B19′ and the characteristic temperatures were close to room temperature. Measurements under a load of 0.02 – 0.3 N revealed an increase in the Vickers microhardness of the molybdenum-implanted surface ($H_V = 440 - 450$ MPa) compared to the unimplanted surface ($H_V = 390$ MPa).

In Ref. 156, the surface layer of $Ni_{50}Ti_{40}Zr_{10}$ alloy was studied before and after implantation of molybdenum ions ($D_1 = 1.8 \times 10^{17}$ and $D_2 = 5 \times 10^{17}$ ion cm$^{-2}$, $E = 50$ keV). It was shown that, in accordance with the dependence of the microhardness $H_V$ on the indenter penetration depth $h$ (μm), the surface area of the indenter imprint into the implanted samples decreases. The $H_V$ values reduced from 450 (at a depth of 0.6 μm) to 390 MPa (at a depth of 1.2 μm). At loads of 0.2 N and higher (this corresponds to the indenter penetration depth from 1 to 2 μm), the microhardness of the implanted samples did not change; this was observed at different implantation doses. It was concluded that the thickness of the modified layer was ~1 μm. At loads ⩾0.1 N, the microhardness was significantly influenced by deeper-lying layers whose microstructure also changed upon ion implantation. This was explained by the so-called long-range effect.

The modified layer is different from the initial material in mechanical properties and structure. This was confirmed by the results of surface fracture studies carried out using implanted and untreated $Ni_{50}Ti_{40}Zr_{10}$ (austenite) samples. The samples were cyclically loaded on a reverse torsion pendulum setup operating in the torsion mode un to fracture by twisting. The single-phase B2 state of the material was attained by maintaining the temperature at 170 °C, above the point of direct martensitic transformation. An analysis of the photomicrographs of surface fracture showed that the virgin samples were characterized by internal stresses along interfaces or grain boundaries. As to the implanted samples, the character of the surface of fracture in the surface layer and adjacent layers suggests a brittle fracture of grains of the B2 phase. The thickness of the sublayer that lies immediately under the modified surface layer is dose-dependent, namely, about 30 μm for the $D_1$ dose and about 90 μm for the $D_2$ dose.

During the tests, the twisting angles were measured after loading – unloading cycle. It was stated[156] that plastic deformation in the implanted samples occurs at lower loads compared to the initial samples. Also, cracking in the implanted samples was found to be 10% – 15% higher than in the untreated samples. Under the action of twisting deformation, samples broke down. The authors[156] believe that an increase in plastic deformation of the B2 phase after ion implantation favours hardening of $Ni_{50}Ti_{40}Zr_{10}$. This was explained by extension of the deformed region, namely, plastic deformation of implanted samples is much larger than that of the starting samples.

Figure 19 presents the results of Vickers microhardness tests of NiTi alloy (austenite phase) before and after implantation of nitrogen ions (dose $1.5 \times 10^{18}$ ion cm$^{-2}$) under different loads.[128] As can be seen, the implanted samples exhibit a decrease in the microhardness in the near-surface layer (~70 μm from surface) at all loads compared to the initial alloy. The effect is most pronounced at the minimal load (0.05 N). The structure and phase composition of the near-surface layer after ion implantation differ from those of the matrix material. The structure of the austenite phase in the near-surface layer is distorted.

Usually, it is impossible to determine the microhardness of shape memory NiTi samples in the austenite phase with certainty because this problem has not been correctly discussed in the literature.[134] Under low loads, the microhardness of shape memory materials can vary over a rather wide range. The microhardness determined from the parameters of the inverted imprint appears to be much higher than the true value. This is due to the fact that under low loads the material exhibits high elastic properties (elastic recovery of the inverted imprint occurs) and therefore, the hardness is overestimated. In this connection, calculations are performed taking into account the size of the deformed region of the material surrounding the imprint from the outside.

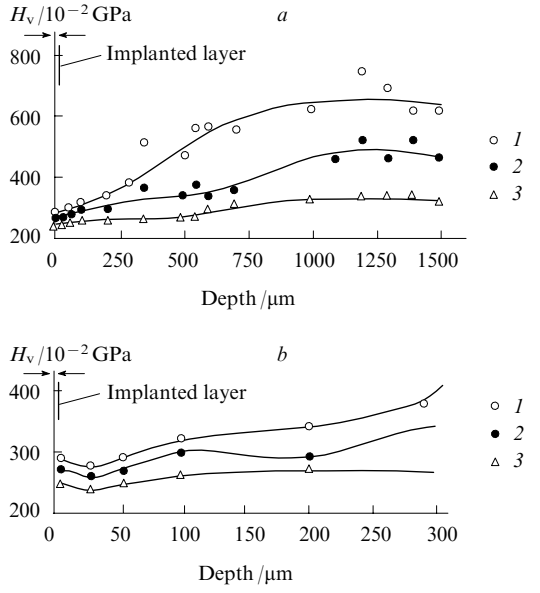



**Fig. 19.** Microhardness of NiTi alloy (austenite) before (*a*) and after (*b*) implantation with nitrogen ions ($D_1 = 1.5 \times 10^{18}$ ion cm$^{-2}$) measured under loads of 0.05 (*1*), 0.1 (*2*) and 0.2 N (*3*).[43, 128]

Note that for the shape memory materials the microhardness values calculated by different authors are usually different and for such materials the classical definition of hardness as the ability of a material to withstand plastic deformation or as a measure of resistance to the action of indenter is not valid. The $H_V$ values do not include the elastic component of deformation. In the case of an elastoplastic material, this causes no large errors because elastic deformations are small. However, for shape memory alloys almost all total deformation is elastic and therefore issues arise concerned with the hardness of the shape memory materials.[134]

Mechanical properties (hardness and Young modulus) of the surfaces of NiTi samples implanted with $N^+$ and $B^+$ ions were studied with a nanoindenter equipped with a diamond tip in Berkovich geometry in a load range from 0.5 to 20 mN.[148] It was shown that by and large, variation of loads and types of implanted ions has little effect on the dependences of the hardness and elastic modulus on the indentation depth. For instance, the elastic modulus of unimplanted NiTi surface is 65 GPa (at a maximal load of 2 mN) and the hardness is 4.2 GPa. After implantation of nitrogen ions accompanied by loading from 0.5 to 2 mN the elastic modulus decreases from 105 to 75 GPa. For implantation of boron ions, the elastic modulus decreases from 110 to 75 GPa. Further loading causes the dependence of the Young modulus to reach a characteristic plateau and to attain a value of 70 GPa for both types of implanted ions at a maximal load of 20 mN. The hardness values for the layers implanted with $N^+$ and $B^+$ ions are somewhat different. For instance, implantation of nitrogen ions accompanied by an increase in the indenter load from 0.5 to 2 mN led to a slight increase in $H$ from 6.5 to 7.6 GPa; however, further loading of the indenter caused the microhardness to gradually decrease to a value of 4.6 GPa attained at the maximal load. No peak was observed for the boron-implanted NiTi samples ($H$ = 7.6 GPa at load of 0.5 mN). On further loading the $H$ value gradually decreases to 4.6 GPa at the maximal load of 20 mN. It is important that changes in the dose of implanted $N^+$ and $B^+$ ions (in particular, for implantation of nitrogen in the doses of $10^{16}$ and $10^{17}$ ion $cm^{-2}$) cause the microhardness to increase; the best result was obtained at a nitrogen ion dose of $5\times10^{16}$ ion $cm^{-2}$. This dose is also optimal for increasing the elastic modulus. For implantation of boron ions, the maximal hardness and elastic modulus values were attained at a dose of $10^{17}$ ion $cm^{-2}$. Changes in the parameters $H$ and $C$ (according to the nanoindentation tests) depending on the ion dose are collected in Table 4 (no depth was indicated). Based on the observed changes in the mechanical properties ($H$, $C$) and on the results of GIXRD studies, it was assumed that hardening of the NiTi surface is mainly due to the formation of a complex system of defects in the crystal lattice after ion implantation.

**Table 4**. Results of microhardness ($H$) and elastic modulus ($C$) measurements for NiTi samples implanted with different doses of boron and nitrogen ions.[148]

| Ion | $D$ /ion $cm^{-2}$ | $c_{max}$ (at.%) | $H$ /GPa | $C$ /GPa |
|---|---|---|---|---|
| – | – | – | 4.2 | 65 |
| $B^+$ | $10^{16}$ | 0.64 | 7.00 | 103 |
| $B^+$ | $5\times10^{16}$ | 3.10 | 7.25 | 95 |
| $B^+$ | $10^{17}$ | 6.01 | 7.70 | 110 |
| $N^+$ | $10^{16}$ | 0.94 | 6.30 | 91 |
| $N^+$ | $5\times10^{16}$ | 4.53 | 7.55 | 104 |
| $N^+$ | $10^{17}$ | 8.66 | 7.30 | 102 |

In the microhardness tests, the indenter imprints on the surface serve a measure of distortions due to the application of indenter. As the temperature is raised above $A_s$, residual stress of NiTi alloy disappears due to the phase transformation. In practice, depending on the stress magnitude and on the heating temperature, no complete shape recovery occurs and the surface still bears some shallower imprints compared to the their depth before heating. Therefore, the shape memory effect can be studied using profilometry measurements and an analysis of shape changes in the indenter imprints during controlled heating of samples.

The heating temperatures and the imprint depths[34] are listed in Table 5. In that study, samples were heated in water. The temperature was maintained with a temperature controller, the indentation depth was measured with a scanning profilometer at a magnification of 5000. Profilometry measurements were carried out at 25 °C (Fig. 21). Three measurements were done for each load value. Based on the results of profilometry measurements, so-called contour maps of the surface were plotted. The shape of the imprints and the imprint profiles at different loads are presented in Figs 20 and 21, respectively.

Interesting results of studies on shape memory materials from the standpoint of changes in the surface state after modification were reported.[118,149] Wear resistance studies of implanted layers involved measurements of the friction coefficient using a ball–plane tester. A tungsten carbide ball 5 mm in diameter was pressed to the sample surface under a load of 1.8 N and then forced to execute oscillatory motion with an amplitude to 100 μm and a frequency of 8 Hz. It was found that for the shot-peened surface containing austenite and martensite phases the lowest friction coefficient at 1000 cycles was obtained at a maximal load of $7\times10^5$ Pa. The initial value of the friction coefficient was the highest (Fig. 22) for the initial martensite samples and remained unchanged until nearly 450 cycles. This result was

**Table 5**. Imprint depth (μm) on the surface of ion-implanted and virgin samples at different loads.[34]

| $T$ /°C | Virgin surface under load /N | | | | | | Ion-implanted surface under load /N | | | | | |
|---|---|---|---|---|---|---|---|---|---|---|---|---|
| | 4 | 7 | 10 | 13 | 16 | 20 | 4 | 7 | 10 | 13 | 16 | 20 |
| 25 | 4.5 | 6.1 | 7.0 | 7.8 | 8.8 | 9.9 | 3.9 | 5.6 | 7.4 | 8.2 | 9.0 | 10.2 |
| 45 | 4.4 | 6.1 | 6.8 | 7.9 | 8.0 | 9.8 | 4.1 | 6.0 | 7.1 | 8.3 | 8.9 | 10.0 |
| 55 | 3.8 | 5.5 | 6.5 | 7.4 | 7.3 | 9.5 | 3.9 | 5.8 | 6.9 | 7.6 | 8.7 | 9.9 |
| 65 | 3.0 | 4.2 | 2.0 | 2.7 | 3.0 | 3.2 | 3.5 | 4.6 | 5.1 | 6.0 | 7.5 | 8.8 |
| 75 | – | – | – | – | 2.8 | 3.3 | – | – | – | – | 4.2 | 5.5 |

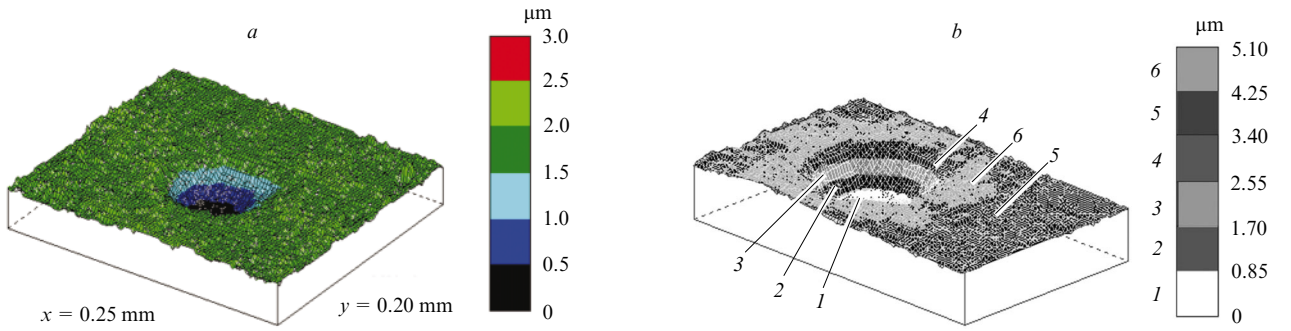



**Fig. 20.** Indenter imprints on the surface derived from the NiTi profilometry measurements under a load of 16 N after heating of the sample to 75 °C: virgin (*a*) and implanted ($D = 10^{18}$ ion cm$^{-2}$, $E = 65$ keV) (*b*) NiTi samples.[34]

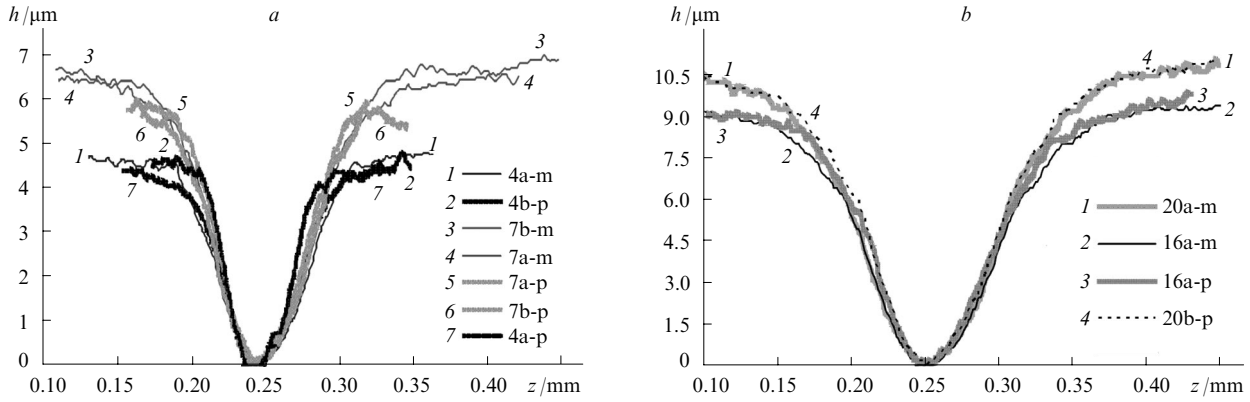



**Fig. 21.** Profiles of indenter imprints on the surface of implanted and virgin samples under loads of 4 and 7 N (*a*) and 16 and 20 N (*b*) obtained at $T = 25$ °C.[43]
Profiles under load (*a*) and under unloading (*b*). Implanted ($10^{18}$ ion cm$^{-2}$, 65 keV) and virgin surfaces are denoted by 'p' and 'm'.

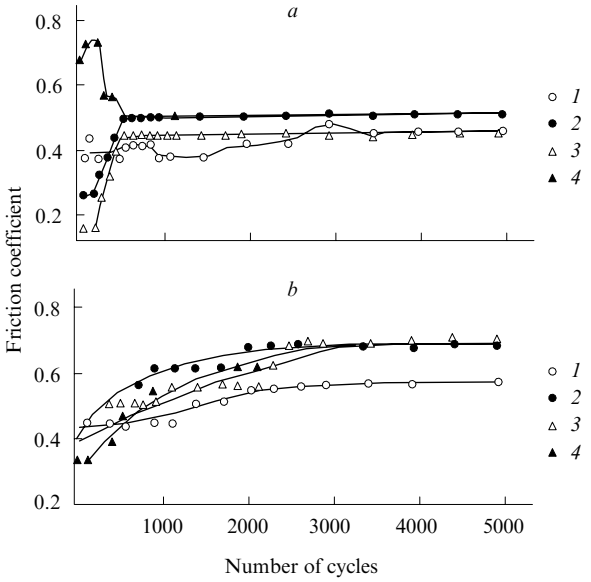



**Fig. 22.** Friction coefficient of NiTi in the austenite and martensite phases plotted *vs.* wear cycles for the virgin material and after shot-peening (*a*) and after implantation with nitrogen ions (*b*).[149]
(*a*) Hardened austenite (*1*), virgin austenite (*2*), hardened martensite (*3*) and virgin martensite (*4*);
(*b*) dose /ion cm$^{-2}$: $10^{18}$ (*1*), $10^{16}$ (*2*), $10^{15}$ (*3*) and $10^{13}$ (*4*).

explained by probable local formation of martensite upon collisions with the surface. As the number of cycles increased, the friction coefficient reached a particular value that subsequently remained unchanged.

The results obtained for the nitrogen-implanted samples suggest that an increase in the ion dose to $10^{18}$ ion cm$^{-2}$ leads to reduction of the friction coefficient; however, the friction coefficient values of the implanted samples change more slowly compared to the shot-peened samples. Samples treated by both methods are characterized by stabilization of the friction coefficient values, namely, after about 1200 test cycles for the shot-peened and after 2500 cycles for the ion-implanted surface. It is believed that implanted surfaces ($D = 10^{18}$ ion cm$^{-2}$) are more wear resistant for less than 2500 test cycles, although the friction coefficient of the mechanically treated surface is usually lower (*e.g.*, 0.3 for shot-peening and 0.43 for ion implantation, both for at most 500 cycles). Unlike the implanted samples, the friction coefficient of the mechanically treated martensite samples remains unchanged in the range from 1000 to 2500 test cycles.

The effect of implantation with nitrogen ions ($D_1 = 10^{17}$ and $D_2 = 2 \times 10^{18}$ ion cm$^{-2}$, $E = 50-65$ keV) on the wear resistance of a shape memory material was studied[150] taking samples of equiatomic NiTi alloy (martensite phase) as examples. The samples $22 \times 5.4 \times 0.3$ mm in size were annealed in a vacuum oven at 583 K for 30 min and

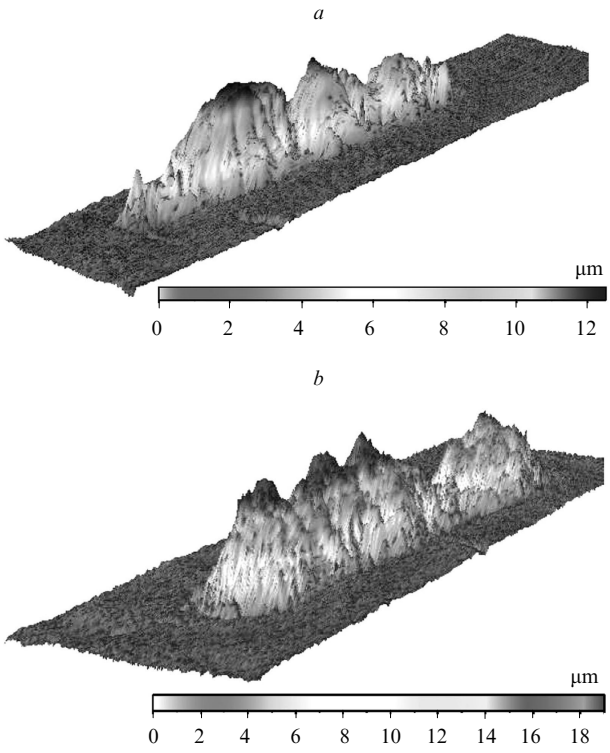



**Fig. 23.** Wear profiles of NiTi alloy: inverted imprints of wear surfaces of virgin NiTi (load 0.4 N, test duration 12 h) (*a*) and implanted NiTi (load 0.7 N, test duration 6 h) (*b*).[43, 150]

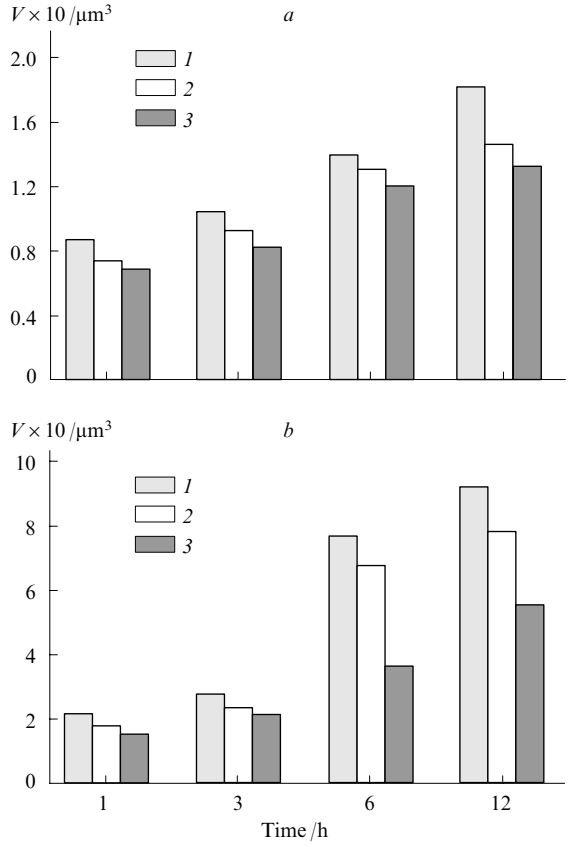



**Fig. 24.** Consumption ($V$) of NiTi alloy before (*1*) and after ion implantation [$D_1 = 10^{17}$ (*2*) and $D_2 = 2 \times 10^{18}$ ion cm$^{-2}$ (*3*), $E = 50-65$ keV] during 'dry sliding' test plotted *vs.* test duration at a load of 0.4 (*a*) and 0.7 N (*b*).[46]

then washed in a solution of 10% $NClO_4 + 90\%$ AcOH. The wear resistance of the surface layer under friction was determined from the results of measurements with a sapphire ball tribotester 6 mm in diameter with a piston sliding (no lubricant!) on the surface of the material. This test was named 'dry piston sliding wear test'. Under the tests, the ball was loaded with 0.4 N and 0.7 N, and the amplitude of reciprocating motion of the ball was 3 mm. The wear resistance was studied using untreated and implanted samples. The test duration was 1, 3, 6 and 12 h. To obtain reproducible results, tests of all samples were repeated three to five times for different loads and test durations. The ball sliding on the surface leaves visible signs of wear (tracks) in the form of grooves. The degree of wear of the material can be evaluated from the depth of the groove using the volume of the groove as a measure of consumption of the material. Also, the wear tests were followed by profilometry measurements of the grooves; this made it possible to compare the surface morphologies. Maps of the surface under study after friction were constructed using the Hommel Map Expert software (Jenoptik, Germany),‡ which allows one to construct inverted images of wear signs on the surface of the material (this serves to observe the 'bottom' of grooves, see Fig. 23).

Implanted samples revealed higher wear resistance of the surface layer compared to untreated samples. The dependence of consumption of NiTi before and after ion implantation ($D_1 = 10^{17}$ and $D_2 = 2 \times 10^{18}$ ion cm$^{-2}$, $E = 50-65$ keV) under 'dry sliding' conditions on time is shown in Fig. 24. Also, the implanted samples were characterized by smaller amounts of consumed NiTi material compared to the unimplanted samples under different loads (0.4 and 0.70 N) at any test duration (1, 3, 6 and 12 h).[46, 150, 153, 157, 158]

Under a lower load (0.4 N, see Fig. 24 *a*) and at the implantation dose $D_2$, the increase in the wear resistance was more pronounced not only compared to the unimplanted samples, but also compared to the samples modified with the lower dose $D_1$. After the 1 h test, the amounts of the consumed NiTi material for all samples differ insignificantly. Considerable differences were observed for the long-term tests.

Improvement of the corrosion resistance of shape memory alloys becomes topical in connection with the wide use of these materials in biomedicine. Usually, NiTi-based alloys exhibit high anti-corrosion properties and biocompatibility. However, the operating lifetime of implants produced from these materials and utilized in corrosive biological media is limited. High content of nickel (allergen and carcinogen) limits the operating lifetime of implants made of NiTi-based alloys. Development of corrosion is known to be dependent on the state of the surface layer.

‡ Documentation can be downloaded from, *e.g.*, http:\\www.teknikel.-com/files/kategori/140/dosya/puruzluluk–ve-kontur-genel-katalog.pdf

This is to a great extent valid for NiTi alloys whose surface contains complex and developed martensite inclusions. Thus, improvement of the corrosion resistance trough surface modification is strongly influenced by the chemical composition of the material.

A corrosive medium was simulated by a mixture 10 ml HF + 30 ml $HNO_3$ + 50 ml $H_2O$ and used for 20-s etching of samples.[117] TEM studies demonstrated a poorer corrosion resistance for the unimplanted material. A comparison of the corrosion resistance of nitrogen-implanted NiTi samples revealed the highest corrosion resistance for the samples implanted with two doses, $10^{17}$ and $5\times10^{17}$ ion cm$^{-2}$ ($E$, = 100 keV). The observed increase in the corrosion resistance upon ion implantation was explained by the appearance of transverse stress in the implanted layer, but no detailed analysis of this effect was performed.

A study[38] on the properties of the surface of implants under the action of corrosive media presented the results of complex investigations of the physicochemical properties of NiTi alloys after implantation with titanium and molybdenum ions as well as qualitative estimates of the corrosion resistance of the modified layers in biological media. Samples under study were made of two or three components, *viz*., $Ti_{49.5}Ni_{50.5}$, $Ti_{50}Ni_{44}Zr_6$, $Ti_{40}Ni_{50}Zr_{10}$, $Ti_{50}Ni_{50-x}Au_x$ ($x$ = 1 at.%, 5 at.%, 10 at.%, 15 at.%, 20 at.%), $Ti_{50}Ni_{50-x}Pd_x$ ($x$ = 2 at.%, 6 at.%, 10 at.%). The initial samples $1\times1\times20$ mm in size were annealed *in vacuo* ($10^{-3}$ Pa) for 1 h at 1073 K, polished with a diamond paste and then with a mixture of composition 10% $HClO_4$ + 90% acetic acid. Ion implantation was carried out using an implanter operating in pulsed mode (pulse repetition frequency was 50 Hz). The $Ti_{49.5}Ni_{50.5}$ samples were implanted with $Ti^+$ ions ($D = 10^{17}$ ion cm$^{-2}$, $E$ = 60 keV) and the $Ti_{50}Ni_{44}Zr_6$ and $Ti_{40}Ni_{50}Zr_{10}$ samples were implanted with $Mo^+$ ions ($D = 2.5\times10^{16}$ and $2.5\times10^{17}$ ion cm$^{-2}$, respectively; $E$ = 60 keV). Qualitative assessment of the corrosion resistance was done gravimetrically. Samples were weighed on an analytic balance with an accuracy of $\pm10^{-5}$ g and their linear dimensions were determined by an optical microscope with an accuracy of $\pm10^{-3}$ mm. The corrosion resistance was determined from the ratio of the mass loss by the sample

$$\Delta m = m_0 - m_1$$

($m_0$ and $m_1$ are the initial and final masses of the sample determined after each measurement) to the total surface area $S$. Tests were performed in two types of corrosive media:

— in 0.99% NaCl solution and

— in blood plasma (9 g litre$^{-1}$ NaCl + 0.42 g litre$^{-1}$ KCl + 0.24 g litre$^{-1}$ $CaCl_2$ + 2 g litre$^{-1}$ $NaHCO_3$ + 2 g litre$^{-1}$ glucose).

Samples were kept at room temperature for 1800 h in the first medium and at 310 K for 3442 h in the second medium. The mass measurements were carried out after 1, 3, 5 and 7 days and then after 2, 3, 4, 6, 8 and 12 weeks. Both implanted and virgin $Ti_{49.5}Ni_{50.5}$ and $Ni_{50}Ni_{44}Zr_6$ samples were tested in the NaCl solution, as well as both implanted and virgin $Ni_{49.5}Ni_{50.5}$ samples were tested in the blood plasma solution. Investigations were carried out over a period of a year and studies of the surface morphology were accompanied by regular mass measurements.

An analysis of changes in the corrosion resistance $\Delta m/S$ with time showed that all samples demonstrated a strong dependence of the change in mass on the chemical composition, duration of storage in solution and on ion implantation parameters (ion type and dose). For all types of treatment, an improved corrosion resistance after ion implantation was observed. The best result was obtained after implantation of molybdenum ions into $Ti_{50}Ni_{44}Zr_6$ ($D_1 = 2.5\times10^{16}$ and $D_2 = 2.5\times10^{17}$ ion cm$^{-2}$). The corrosion resistance of the implanted samples appeared to be almost twice as high as that of the unimplanted samples. Metallographic studies substantiated the results obtained. An optical microscopy study of virgin samples demonstrated signs of pitting corrosion at grain boundaries. Photomicrographs of implanted samples showed that the surface state was almost unchanged. Increased corrosion resistance of implanted samples was explained using the results of a study of the chemical composition by Auger electron spectroscopy. Namely, implantation of titanium ions led to the formation of a nickel-free oxide layer ~20 nm thick on the surface. In the virgin samples, the surface oxide layer was ~10 nm thick and contained ~20 at.% Ni. Implanted samples were characterized by the formation of a specific oxide sublayer with minimal content of nickel (only at a depth of baout 50 nm from the surface the nickel concentration values appeared to be typical). It was concluded that the decisive factor in improvement of the corrosion resistance is the lack (or low content) of nickel in the modified surface layer.§ A beneficial effect of high implantation doses of $Ti^+$ and $Mo^+$ ions on the corrosion properties of NiTi-based alloys was thus substantiated.[38] This makes application of these materials in medicine feasible.

It should also be noted that at these implantation doses, the concentration of implanted ions was at most 1 at.%. Therefore, improvement of the physicomechanical properties is solely due to the formation of carbonitride or oxycarbide layers that act as protective layers.[157, 158]

## VII. Conclusion

Metallic alloys with thermoelastic martensitic transformations and the shape memory effect due to these transformations are bright representatives of new-generation materials. The top position in this class of materials is occupied by titanium nickelide alloys that exhibit high mechanical and plastic properties, unique (singly and multiply reversible) shape memory effect, thermomechanical and thermal cycle reliability, as well as long operating life, high heat resistance, corrosion resistance and biocompatibility. They have simple chemical compositions, can be produced with ease and subsequent processing operations aimed at

§ Implantation of titanium ions leads to formation of Ti-rich surface layers in the alloy and to the appearance of barrier layers that separate nickel from the environment. It was found that the ion-modified barrier layers had different chemical composition and thickness depending on the pretreatment of the surface of NiTi substrate. Changes in the chemical composition manifested themselves as separation of the near-surface layer into external and internal layers. The external layer contained titanium and almost no nickel, was oxygen-rich and had a more homogeneous compositional depth profile compared to the ion-modified layer formed on the electrochemically treated NiTi substrate.

forming wires, strips, sheets and intricate shapes are also simple. This predetermines the advantages of NiTi shape memory alloys over other materials and great prospects for their application in the future.

Presently, utilization of shape memory alloys is widely discussed. Some fields of practical applications of these materials include:

— industrial equipment: elements of starting systems and actuators (for, *e.g.*, temperature triggering to close the tank valves or valves of solid waste containers), thermal switches, fuses for communication lines, elements of aerials for mobile network operators, recorders, valve bodies, *etc.*;

— automotive industry: valves, vibration damping gaskets, starting mechanisms, *etc.*;

— aerospace industry: connectors and materials for transformable antenna systems, solar cell batteries and systems for intellectual airfoil geometry variation to reduce vibrations;

— electronics: microsensors, energy-absorbing devices, temperature and pressure control systems;

— medicine: implants, vasodilators, blood filters, orthopedic plates, surgical forceps, endoscopes, dental appliances, *etc*.

In this review, we have shown that ion implantation significantly influences the physicomechanical properties of shape memory materials and phase transformation in them. At high implantation doses, the physicomechanical properties of samples or articles made of NiTi can be significantly improved; in some cases, nanocrystalline surface (or near-surface) layers can form.[50, 159 – 162] It should be noted that to date, there are a relatively few publications on implantation of shape memory materials with metal ions and on double implantation of metal and gas ions. Taking into account great prospects for applications of shape memory materials, one can hope for continuation of research in the field.

This review has been written with the financial support from the Ministry of Education and Science of Ukraine (State-Financed Research Project Nos 0110U001257 and 0112U001382) and the Ministry of Education and Science of the Russian Federation (State Contract No. 15521170876).

The authors are grateful to the staff of the Department of Materials for Reactor Building and Physical Technologies (School of Physics and Technology, V N Karazin Kharkiv National University, Ukraine) for criticism and suggestion.

The authors express their gratitude to L L Meisner, A I Lotkov and A A Nejman (Institute of Strength Physics and Materials Science, Siberian Branch of the Russian Academy of Sciences, Tomsk, Russian Federation) for kindly providing reprints on the title subject.

## References

1. J Van Humbeeck *Scr. Mater.* **50** 179 (2004)
2. J Van Humbeeck *Mater. Sci. Eng. A* **273** 134 (1999)
3. S Shabalovskaya, J Anderegg, J Van Humbeeck *Acta Biomater.* **4** 447 (2008)
4. B Raniecki, Ch Lexcellent *Eur. J. Mech. A: Solids* **17** 185 (1998)
5. X Zhao, W Cai, L Zhao *Surf. Coat. Technol.* **155** 236 (2002)
6. S Moyne, C Poilane, K Kitamura, S Miyazaki, P Debobelle, C Lexcellent *Mater. Sci. Eng. A* **273 – 275** 727 (1999)
7. J E Elder, R Thamburaj, P C Patniak *Surf. Eng.* **5** 55 (1989)
8. T Wierzchoń, E Czarnowska, D Krupa *Inzynieria Powierzchni w Wytwarzaniu Biomateriałów Tytanowych* (Warszawa: Oficyna Wydawnicza Politechniki Warszawskiej, 2004)
9. V C Nath, D K Sood, R R Manory *Surf. Coat. Technol.* **49** 510 (1991)
10. I I Kornilov, O K Belousov, E V Kachur *Nikelid Titana i Drugie Splavy s Effektom 'Pamyati'* (Nickel Titanium and Other Alloys with Memory Effect) (Moscow: Nauka, 1977)
11. V A Likhachev, S L Kuz'min, Z P Kamentseva *Effekt Pamyati Formy* (Effect of 'Shape Memory' (Leningrad: Leningrad State University, 1987)
12. K Otsuka, Y Suzuki, K Shimizu, Y Sekiguchi, G Tadaki, T Honma, S Miyazaki *Shape Memory Alloys* (Ed. H Funakubo) (New York: Gordon and Breach, 1987)
13. *Shape Memory Materials* (Eds K Otsuka, C M Wayman) (Cambridge: Cambridge University Press, 1999)
14. V N Khachin, V G Pushin, V V Kondrat'ev *Nikelid Titana: Struktura i Svoistva* (Titanium Nickelide: Structure and Properties) (Moscow: Nauka, 1992)
15. V G Pushin, S D Prokoshkin, R Z Valiev *Splavy Nikelida Titana s Pamyat'yu Formy. Struktura, Fazovye Prevrashcheniya i Svoistva* (Shape Memory Titanium Nickelide Alloys. Structure, Phase Transformations and Properties) (Ed. V G Pushin) (Ekaterinburg: Ural Branch of the Russian Academy of Sciences, 2006) Pt. 1
16. *Materialy s Effektom Pamyati Formy: Spravochnoe Izdanie v Chetyrekh Tomakh* (Shape Memory Materials: Handbook in Four Volumes) (Ed. V A Likhachev) (St Petersburg: Research Institute of Chemistry, St Petersburg State University, 1997)
17. *Meditsinskie Materialy i Implantaty s Pamyat'yu Formy. Meditsinskie Materialy s Pamyat'yu Formy* (Medical Materials and Implants with Shape Memory. Shape Memory Medical Materials) (Ed. V E Gyunter) (Tomsk: MITs, 2011) Vol. 1
18. C B Mello, M Ueda, C M Lepienski, H Reuther *Appl. Surf. Sci.* **256** 1461 (2009)
19. C B Mello, M Ueda, M M Silva, H Reuther, L Pichon, C M Lepienski *Wear* **267** 867 (2009)
20. N Padhy, S Ningshen, B K Panigrahi, U Kamachi Mudali *Corros. Sci.* **52** (1) 104 (2010)
21. S Aoki, Y Teranishi, A Mitsuo, M Kawaguchi, K Morikawa, A Suzuki, M Masuko *J. Eng. Tribol.* **224** 957 (2010)
22. K Feng, X Cai, Z Li, P K Chu *Mater. Lett.* **68** 450 (2012)
23. N Kumar, S Kataria, S Dash, S K Srivastava, C R Das, P Chandramohan, A K Tyagi, K G M Nair, B Raj *Wear* **274 – 275** 60 (2012)
24. P Saravanan, V S Raja, S Mukherjee *Surf. Coat. Technol.* **201** 8131 (2007)
25. B Raniecki *Thermomechanics of Pseudoelasticity of Shape Memory Materials* (Ed. W K Nowacki) (Warsaw: IPPT PAN, 1996) Vol. 1, Ch. 2, p 55
26. D Stroz *Oddziaływanie Zniekształceń Sieciowych na Przebieg Przemiany Martenzytycznej w Stopach NiTi* (Katowice: Wydawnictwo Uniwersytetu Śląskiego, 2005)
27. L G Machado, M A Savi *Braz. J. Med. Biol. Res.* **36** 683 (2003)
28. R Pelton, D Stockel, T W Duerig *Mater. Sci. Forum* **63** 327 (2000)
29. B Raniecki, Ch Lexcellent, K Tanaka *Arch. Mech.* **44** 261 (1992)
30. E A Bazyl, A D Pogrebnjak, S V Sokolov, N V Sviridenko *Fiz. Khim. Obrab. Mater.* **1** 17 (2000)

31. A D Pogrebnjak, A P Kobzev, B P Gritsenko, S Sokolov, E Bazyl, N V Sviridenko, A N Valyaev, Yu F Ivanov *J. Appl. Phys.* **87** 2142 (2000)
32. A D Pogrebnjak, A P Kobzev, B P Gritsenko, S Sokolov, E Bazyl, N V Sviridenko, A N Valyaev, S V Plotnikov *Jpn. J. Appl. Phys.* **38** L248 (1999)
33. L L Meisner, A I Lotkov, M G Dementyeva, N N Koval, Yu F Ivanov, E Yu Gudimova *Rare Met.* **28** 361 (2009)
34. N Levintant-Zayonts, S Kucharski *Mater. Eng.* **34** 855 (2011)
35. H Gleiter *Acta Mater.* **48** 1 (2000)
36. V V Brazhkin, A G Lyapin, R J Hemley *Philos. Mag. A* **82** 231 (2002)
37. N N Cherenda, V V Uglov, M G Poluyanova, V M Astashynski, A M Kuzmitski, A D Pogrebnjak, B Stritzker *Plasma Proc. Polym.* **6** (Suppl. 1) S178 (2009)
38. L L Meisner, I V Nikonova, A I Lotkov, V V Razdorskii, M V Kotenko *Perspekt. Mater.* **3** 1 (2008)
39. L L Meisner, A I Lotkov, A A Neiman, G V Arysheva *Perspekt. Mater.* **13** 572 (2011)
40. Y Li, S Wei, X Cheng, T Zhang, G Cheng *Surf. Coat. Technol.* **202** (13) 3017 (2008)
41. N Ikenaga, Y Kishi, Z Yajima, N Sakudo, Sh Nakano, H Ogiso *Nucl. Instrum. Meth. B* **267** 1509 (2009)
42. Y F Zheng, D Liu, X L Liu, L Li *Appl. Surf. Sci.* **255** 512 (2008)
43. N Levintant-Zayonts, Ph.D. Thesis, Institute of Fundamental Technological Research PAS, Warsaw, 2009
44. F F Komarov *Ionnaya Implantatsiya v Metally* (Ion Implantation in Metals) (Moscow: Metallurgiya, 1990)
45. K K Kadyrzhanov, F F Komarov, A D Pogrebnyak, V S Rusakov, T E Turkebaev *Ionno-Luchevaya i Ionno-Plazmennaya Modifikatsiya Materialov* (Ion-Beam and Ion-Plasma Modification of Materials) (Moscow: Moscow State University, 2005)
46. O Yaskiv, I Pohreliuk, V Fedirko, T Kravchyshyn, O Bonchyk, N Levintant-Zayonts *Mater. Eng.* **29** 134 (2008)
47. E Leitao, C Sa, R A Siilva, M A Barbosa *Corros. Sci.* **11** (37) 1861 (1995)
48. *Ion Implantation* (Ed. J K Hirvonen) (New York: Academic Press, 1980)
49. N A Azarenkov, V M Beresnev, A D Pogrebnjak, D A Kolesnikov *Nanostrukturnye Pokrytiya i Nanomaterialy: Osnovy Polucheniya. Svoistva. Oblasti Primeneniya: Osobennosti Sovremennogo Nanostrukturnogo Napravleniya v Nanotekhnologii* (Nanostructure Coating and Nanomaterials: Foundations of the Production. Properties. Application Areas: Features of Modern Nanostructure Area in Nanotechnology) (Moscow: URSS, 2012)
50. O M Ivasishin, A D Pogrebnjak, S N Bratushka *Nanostructured Layers and Coating Formed by Ion-Plasma Fluxes in Titanium Alloys and Steels* (Kyiv: Akademperiodyka, 2011)
51. A D Pogrebnjak, S N Bratushka, N Levintant *Przegląd Elektrotechniczny (Electr. Rev.)* **84** (3) 191 (2008)
52. A D Pogrebnjak, O G Bakharev, N A Pogrebnjak Jr, Yu V Tsvintarnaya, V T Shablja, R Sandrik, A Zecca *Phys. Lett. A* **265** 225 (2000)
53. D Krupa, J Baszkiewicz, J A Kozubowski, A Barcz, J W Sobczak, A Biliński, M Lewandowska-Szumieł, B Rajchel *Vacuum* **63** 715 (2001)
54. I Tsyganov, E Wieser, W Matz, H Reuther, E Richter *Surf. Coat. Technol.* **158 – 159** 318 (2002)
55. Z W Kowalski, J Wilk, J Martan *Vacuum* **83** S208 (2009)
56. A D Pogrebnjak, E A Basyl *Vacuum* **64** 1 (2001)
57. A D Pogrebnjak, S N Bratushka, V V Uglov, N K Erdybaeva, V S Rusakov, V M Beresnev, V M Anischik, L V Malikov, N Levintant, P Zukovski *Vacuum* **83** (6) S241 (2009)
58. S M Duvanov, A G Balogh *Nucl. Instrum. Methods B* **171** 475 (2000)
59. S Mandl *Surf. Coat. Technol.* **201** 6833 (2007)
60. N Shevchenko, M-T Pham, M F Maitz *Appl. Surf. Sci.* **235** 126 (2004)
61. A I Lotkov, L L Meisner, V N Grishkov *Fiz. Met. Metalloved.* **99** (2) 1 (2005) [a]
62. O G Bakharev, A D Pogrebnjak, E A Bazyl', S V Sokolov *Metallofiz. Noveish. Tekhnol.* **21** (8) 61 (1999)
63. F F Komarov, A A Komarou, P Zukowski, Cz Karwat, J Sielanko, Cz Kozak, K Kiszczak *Vacuum* **70** 215 (2003)
64. L L Meisner, V P Sivokha, A I Lotkov, E G Barmina, Yu L Giryakova *Materialovedenie* (4) 43 (2003)
65. V A Shulov, A I Ryabchikov, A B Belov, A G Paikin, L V Prokhodtseva *Fiz. Khim. Obrab. Mater.* (2) 33 (2007)
66. A M Smyslov, A A Bybin, R R Nev'yantseva *Fiz. Khim. Obrab. Mater.* (3) 29 (2007)
67. S N Zvonkov, S N Korshunov, Yu V Martynenko, I D Skorlupkin *Pis'ma Zh. Eksp. Teor. Fiz.* **94** 116 (2011) [b]
68. I A Kurzina, I A Bozhko, M P Kalashnikov, Yu P Sharkeev, E V Kozlov *Izv. Akad. Nauk, Ser. Fiz.* **72** 1191 (2008) [c]
69. I A Kurzina *Materialovedenie* (2) 49 (2010)
70. O V Sobol', A A Andreev, S N Grigor'ev, V F Gorban', M A Volosova, S V Aleshin, V A Stolbovoi *Metallov. Term. Obrab. Met.* (4) 43 (2012)
71. V V Stolyarov *Izv. Akad. Nauk, Ser. Fiz.* **76** 108 (2012) [c]
72. Y Cheng, Y F Zheng *Surf. Coat. Technol.* **201** 4909 (2007)
73. K W K Yeung, R W Y Poon, X M Liu, P K Chu, C Y Chung, X Y Liu, S Chan, W W Lu, D Chan, K D K Luk, K M C Cheung *Surf. Coat. Technol.* **201** 5607 (2007)
74. R W Y Poon, J P Y Ho, X Liu, C Y Chung, P K Chu, K W K Yeung, W W Lu, M C Kenneth *Thin Solid Films* **488** 20 (2005)
75. R W Y Poon, J P Y Ho, X Liu, C Y Chung, P K Chu, K W K Yeung, W W Lu, M C Kenneth *Mater. Sci. Eng. A* **390** 444 (2005)
76. H Tollefsen, S Raaen *J. Appl. Phys.* **105** 123501 (2009)
77. L M Pérez, M Arruebo, S Irusta, L Gracia-Villa, J Santamaría, J A Puértolas *Microporous Mesoporous Mater.* **98** 292 (2007)
78. W M Huang, Z Ding, C C Wang, J Wei, Y Zhao, H Purnawali *Mater. Today* **13** (7) 54 (2010)
79. I A Kurzina, E V Kozlov, Yu P Sharkeev, A I Ryabchikov, I B Stepanov, I A Bozhko, M P Kalashnikov, D O Sivin, S V Fortuna *Surf. Coat. Technol.* **201** 8463 (2007)
80. Y Liu, X Zu, Sh Qiu, X Huang *Rare Met.* **25** (6, Suppl. 1) 309 (2006)
81. F Berberich, W Matz, U Kreissig, E Richter, N Schell, W Moller *Appl. Surf. Sci.* **179** 13 (2001)
82. C Díaz, J Lutz, S Mändl, J A García, R Martínez, R J Rodríguez, J J Damborenea, M A Arenas, A Conde *Phys. Status Solidi, C* **5** 947 (2008)
83. L Tan, R A Dodd, W C Crone *Biomaterials* **24** 3931 (2003)
84. H Ji, L Xia, X Ma Y Sun *Wear* **246** 40 (2000)
85. K W K Yeung, R W Y Poon, X Y Liu, J P Y Ho, C Y Chung, P K Chu, W W Lu, D Chan, K M C Cheung *J. Biomed. Mater. Res., Part A* **75** 256 (2005)
86. D-H Kim, H-E Kim, K-R Lee, Ch-N Whang, I-S Lee *Mater. Sci. Eng. C* **22** 9 (2002)

87. K S Kim, K K Jee, Y B Kim, W Y Jang, S H Han *Eur. Phys. J. Spec. Top.* **158** 67 (2008)
88. Yu I Golovin *Fiz. Tv. Tela* **50** 2113 (2008) [d]
89. S Dhara *Solid State Mater. Sci.* **32** 1 (2007)
90. J Luo *Solid State Mater. Sci.* **32** 67 (2007)
91. Y Cheng, Y F Zheng *Mater. Sci. Eng., A* **438 – 440** 1146 (2006)
92. A D Pogrebnjak, V I Bojko, V I Lavrent'yev, A N Valyayev *Met. Phys. Adv. Technol.* **17** 1043 (1999)
93. A D Pogrebnjak, S Bratushka, V I Boyko, I V Shamanin, Yu V Tsvintarnaya *Nucl. Instrum. Metods.* **145** 373 (1998)
94. A D Pogrebnjak, A N Valyaev, O G Bakharev, V V Sushko, S Bratushka, A D Mikhaliov, Yu F Ivanov, V P Rotstein *Surf. Coat. Technol.* **99** 98 (1998)
95. V I Lavrent'ev, A D Pogrebnjak *Surf. Coat. Technol.* **99** 24 (1998)
96. Yu F Ivanov, A D Pogrebnjak, V I Lavrentev *Met. Phys. Adv. Technol.* **16** 1027 (1997)
97. V I Lavrent'ev, A D Pogrebnjak *Phys. Met. Metallogr.* **84** (6) 5 (1997) [a]
98. V I Lavrent'ev, A D Pogrebnyak *Met. Phys. Adv. Technol.* **16** (11) 1233 (1997)
99. V I Lavrent'ev, A D Pogrebnjak, R Sandrik *J. Exp. Theor. Phys. Lett.* **65** (1) 91 (1997)
100. A D Pogrebnjak, S M Duvanov, A D Mikhaliov, V I Lavrentiev, V V Stayko, A V Markov, Yu F Ivanov, D I Proskurovsky *Surf. Coat. Technol.* **89** 90 (1997)
101. Yu F Ivanov, A D Pogrebnjak, V I Lavrent'yev *Met. Phys. Adv. Technol.* **18** 43 (1996)
102. A D Pogrebnyak, L V Malikov, S N Bratushka, N K Erdybaeva, N Levintant, S V Plotnikov *Zh. Tekh. Fiz.* **54** 667 (2009) [a]
103. T Lagrange, C Abromeit, R Gotthardt *Mater. Sci. Eng., A* **438 – 440** 521 (2006)
104. A N Valyaev, M K Kylyshkanov, A D Pogrebnjak, A A Valyaev, S V Plotnikov *Vacuum* **58** 53 (2000)
105. A D Pogrebnjak, V S Ladysev, N A Pogrebnjak, A D Michaliov, V T Shablya, A N Valyaev, A A Valyaev, V B Loboda *Vacuum* **58** 45 (2000)
106. A D Pogrebnjak, N I Shumakova *Surf. Coat. Technol.* **122** 183 (1999)
107. V I Boiko, A N Valyaev, A D Pogrebnjak *Usp. Fiz. Nauk* **169** 1243 (1999) [f]
108. E A Bazyl', A D Pogrebnjak, B P Gritsenko, S V Sokolov, V V Stayko, N V Sviridenko, S N Bratushka *Tech. Phys. Lett.* **25** 621 (1999)
109. Yu N Tyurin, A D Pogrebnjak *Surf. Coat. Technol.* **111** 269 (1999)
110. Yu F Ivanov, A D Pogrebnyak *Met. Phys. Adv. Technol.* **20** 30 (1998)
111. A D Pogrebnjak, V T Shablia, N A Pogrebnjak, R Sandrik, A Zecca, S N Bratushka *Surf. Coat. Technol.* **110** 35 (1998)
112. A D Pogrebnjak, R Sandrik, A D Mikhaliov, N A Pogrebnjak Jr, Yu V Tsvintarnaya, V I Lavrentiev, M Iljashenko, A Zecca *Phys. Lett. A* **241** 357 (1998)
113. V I Lavrent'ev, A D Pogrebnyak, A D Mikhalev, N A Pogrebnjak, R Shandrik, A Zecca, Yu V Tsvintarnaya *Tech. Phys. Lett.* **24** 334 (1998)
114. J Dutkiewicz, W Maziarz, T Czeppe, L Litynska, W Nowacki, P Gadaj, J Lukner, E Pieczyska *Eur. Phys. J.* **158** 59 (2008)
115. C HeBing, J Frenzel, M Pohl, S Shabalovskaya *Mater. Sci. Eng. A* **486** 461 (2008)
116. A V Belyi, V A Kukarenko, V I Kopylov, Yu P Sharkeev *Tren. Iznos* **29** 571 (2008) [g]
117. L Meisner, A Lotkov, V Sivokha, A Turova, E G Barmina *Fiz. Khim. Obrab. Mater.* (1) 78 (2003)
118. J Narojczyk, Z Werner, M Barlak, D Morozow *Vacuum* **83** S228 (2009)
119. X Liu, Sh Wu *Mater. Sci. Eng. A* **444** 192 (2007)
120. X Ju, H Dong *Surf. Coat. Technol.* **201** 1542 (2006)
121. H F Zhang, Y Cheng, Y F Zheng *Surf. Coat. Technol.* **201** 6857 (2007)
122. P Zukowski, F F Komarov, Cz Karwat, K Kiszczak, Cz Kozak, A S Kamyshan *Vacuum* **83** S204 (2009)
123. J Li, M Sun, X Ma, G Tang *Wear* **261** 1247 (2006)
124. M Ueda, M M Silve, C Otani, H Reuther, M Yatsuzuka, C M Lepienski, L A Berni *Surf. Coat. Tech.* **169 – 170** 408 (2003)
125. N Levintant *Vacuum* **81** 1183 (2007)
126. T Czeppe, N Levintant-Zayonts, Z Swiatek, M Michalec *Vacuum* **83** S214 (2009)
127. M Mayer *Nucl. Instum. Methods, B* **266** 1852 (2008)
128. N Levinatnt-Zayonts, S Kucharski *Vacuum* **83** S220 (2009)
129. W Yan, Q Sun, Xi-Qiao Feng, L Qian *Int. J. Solid. Struct.* **44** 1 (2007)
130. S Kucharski, D.Sc. Thesis, Institute of Fundamental Technological Research PAS, Warszawa, 2002
131. S Kucharski, Z Mroz *Mater. Sci. Eng. A* **379** 448 (2004)
132. N Levintant-Zayonts, S Kucharski *Mater. Eng.* **1** 45 (2009)
133. A Ziołkowski, D.Sc. Thesis Institute of Fundamental Technological Research PAS, Warszawa, 2006
134. F T Cheng *Mater. Sci. Technol.* **20** (6) 700 (2004)
135. E Pieczyska, D.Sc. Thesis, Institute of Fundamental Technological Research PAS, Warszawa, 2008
136. K Tanaka, K Kitamura, S Miyazaki *Arch. Mech.* **51** 785 (1999)
137. A Ziołkowski, Ph.D. Thesis, Institute of Fundamental Technological Research PAS, Warszawa, 1995
138. H Pokhmurska, O Kalakhan, H Okhota, N Levintant-Zayonts, in *Proceedings of the European Corrosion Congress (EUROCORR 2008), Edinburg, UK, 2008* p. 7
139. F Auricchio, R Taylor *Comput. Methods Appl. Mech.* **143** 175 (1997)
140. V A L'vov, A A Rudenko, V A Chernenko, E Cesari, J Pons, T Kanomata *Mater. Trans.* **46** 790 (2005)
141. K Otsuka, X Ren *Prog. Mater. Sci.* **50** 511 (2005)
142. P Sitner, Y Liu, V Novak *J. Mech. Phys. Solids* **53** 1719 (2005)
143. D S Plant, D M Grant, L Lea *Biomaterials* **26** 5359 (2005)
144. J Poate, G Foti, D Jacobson *Surface Modification and Alloying* (New York: Plenum, 1983)
145. D J Wever, A G Veldhuizen, M M Sanders, J M Schakenrad, J R van Horn *Biomaterials* **18** 1115 (1997)
146. L L Meisner, V P Sivokha, N A Litovchenko, A A Neiman, S N Meisner, Ch Dyan' *Zh. Fiz. Khim.* **1** (2) 58 (2007) [h]
147. T Asaoka, A Mitsuo *Mater. Trans. JIM* **41** (6) 739 (2000)
148. H Pelletier, D Muller, P Mille, J Grob *Surf. Coat. Technol.* **158 – 159** 309 (2002)
149. D Grant, S Green, J Wood *Acta Metall. Mater.* **43** 1045 (1995)
150. Z Swiatek, M Michales, N Levintant-Zayonts, J Bonarskij, A Budziak, O Bonchyk, G Savitskij *Acta Phys. Pol., A* **120** (1) 75 (2011)
151. L Mejsner, V Sivokha, A Lotkov, E Barmina *J. Phys. IV (France)* **112** 663 (2003)
152. S Green, D Grant, J Wood, A Johanson, L Sarholt-Kristensen *J. Mater. Sci. Lett.* **12** 618 (1993)

153. M Mayer *SIMNRA User's Guide. Tech. Rep. IPP 9/113* Max-Planck-Institut für Plasmaphysik Garching 1997
154. A D Pogrebnjak, N Levintant, L V Malikov, V M Beresnev, S N Bratushka, N K Erdybaeva, T Czeppe, Zb Zwiatek, M Micleales *Vopr. Atom. Nauki Tekh.* (6) 162 (2009)
155. B Raniecki, K Tanaka *Int. J. Eng. Sci.* **32** 1845 (1994)
156. L Meisner, V Sivokha, Yu Sharkeev, S Kul'kov, V Gritsenko *Zh. Tekh. Fiz.* **70** 32 (2000) [e]
157. A D Pogrebnjak, N K Erdybaeva, L V Malikov, S N Bratushka, N Levintant *Vopr. Atom. Nauki Tekh.* (1) 81 (2008)
158. A Pogrebnjak, S Bratushka, N Levintant-Zayonts *J. Nano- Electron. Phys.* **5** 01016 (2013)
159. G A Malygin *Usp. Fiz. Nauk* **181** 1129 (2011) [f]
160. G A Malygin *Fiz. Tv. Tela* **50** 1480 (2008) [d]
161. R A Andrievskii, A M Glezer *Usp. Fiz. Nauk* **179** 337 (2009) [f]
162. K M Zhang, J X Zou, T Grosdidier *J. Nanomater.* ID 978568 (2013)

[a] — *Phys. Met. Metallogr. (Engl. Transl.)*
[b] — *J. Exp. Theor. Phys. Lett. (Engl. Transl.)*
[c] — *Bull. Russ. Acad. Sci., Phys. (Engl. Transl.)*
[d] — *Phys. Solid. State (Engl. Transl.)*
[e] — *Tech. Phys. (Engl. Transl.)*
[f] — *Physics-Uspekhi (Engl. Transl.)*
[g] — *Frict. Wear (Engl. Transl.)*
[h] — *Russ. J. Phys. Chem., Ser. A (Engl. Transl.)*